Technical Report

457

The Microwave System of the Haystack Planetary Radar

C. W. Jones

23 October 1968

Prepared under Electronic Systems Division Contract AF 19(628)-5167 by

Lincoln Laboratory
MASSACHUSETTS INSTITUTE OF TECHNOLOGY
Lexington, Massachusetts

The work reported in this document was performed at Lincoln Laboratory, a center for research operated by Massachusetts Institute of Technology, with the support of the U.S. Air Force under Contract AF 19(628)-5167.

MASSACHUSETTS INSTITUTE OF TECHNOLOGY

LINCOLN LABORATORY

THE MICROWAVE SYSTEM OF THE HAYSTACK PLANETARY RADAR

C. W. JONES

Group 46

TECHNICAL REPORT 457

23 OCTOBER 1968

LEXINGTON MASSACHUSETTS

ABSTRACT

The microwave system of the Haystack Planetary Radar is described and performance data presented. A detailed description of techniques and components is included for those cases which are not representative of common usage or where the state of the art has been advanced.

Accepted for the Air Force
Franklin C. Hudson
Chief, Lincoln Laboratory Office

CONTENTS

THE MICROWAVE SYSTEM OF THE HAYSTACK PLANETARY RADAR

I. INTRODUCTION

The X-band planetary radar at Haystack was inspired by Shapiro's[1-3] suggestion that the general theory of relativity might be checked by a fourth test. He proposed that a radar beam be passed close to the sun and changes in the velocity of propagation due to gravitational retardation be measured by using the echoes from the planets Venus and Mercury.

A conventional pulsed radar which could detect either Venus or Mercury at superior conjunction would require about 50 MW of peak power at X-band. This was far beyond anything that seemed achievable. However, the achievement of 500 kW CW at X-band did appear to be within the state of the art, because Eimac, now a division of Varian Associates, had, in 1964, been successful in a laboratory demonstration of 500 kW CW from a single tube for a short period of time. An industry-wide competition resulted in the choice of a pair of Varian VA-949AM, 250 kW klystrons to power the radar.

The radar system to be used, sometimes erroneously called a CW radar, was to employ a very long pulse, the pulse length being nearly equal to twice the distance between the earth and the target planet. This long pulse was coded in such a way as to allow achievement of the same degree of range resolution as might be obtained using a more conventional pulsed radar.

In order to detect Venus or Mercury at superior conjunction with a sufficient signal-to-noise ratio to allow an accurate determination of range, the microwave system employed with the Haystack antenna must have a transmitter power of 500 kW CW, and a system noise temperature of 75°K. Considering the radome losses, transmission line losses and the estimated noise background when looking in the vicinity of the sun, the low noise receiver must have a flange temperature of less than 25°K in order to achieve the required overall system temperature. With these RF system parameters, the Haystack system threshold (signal = noise in a 1-Hz filter) would be 355 dB.

II. GENERAL DESCRIPTION OF MICROWAVE SYSTEM

The planetary radar, as the microwave equipment for performing the "fourth test" is called, is packaged in an 8- by 8- by 12-foot module which mounts behind the apex of the 120-foot Haystack parabolic reflector.[4] This module, which is referred to as the PR (Planetary Radar) box, can be removed from the antenna and operated at a test position on the ground when the antenna is being used for other purposes. However, the turn-around time for changing equipment boxes is long enough for such changes to be made infrequently.

In order to ensure efficient utilization of the Haystack facility, the RF system has been configured so that the planetary radar equipment may be used for short pulse moon mapping

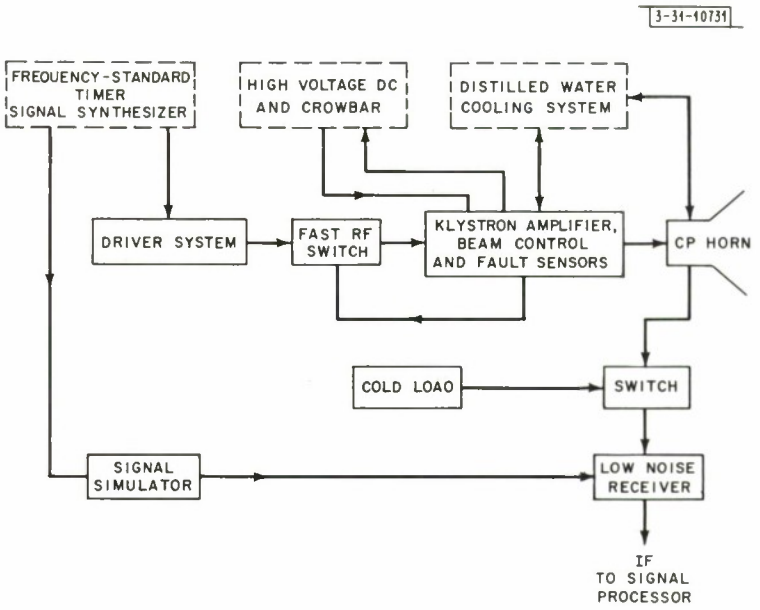

Fig. 1. Basic radar system.

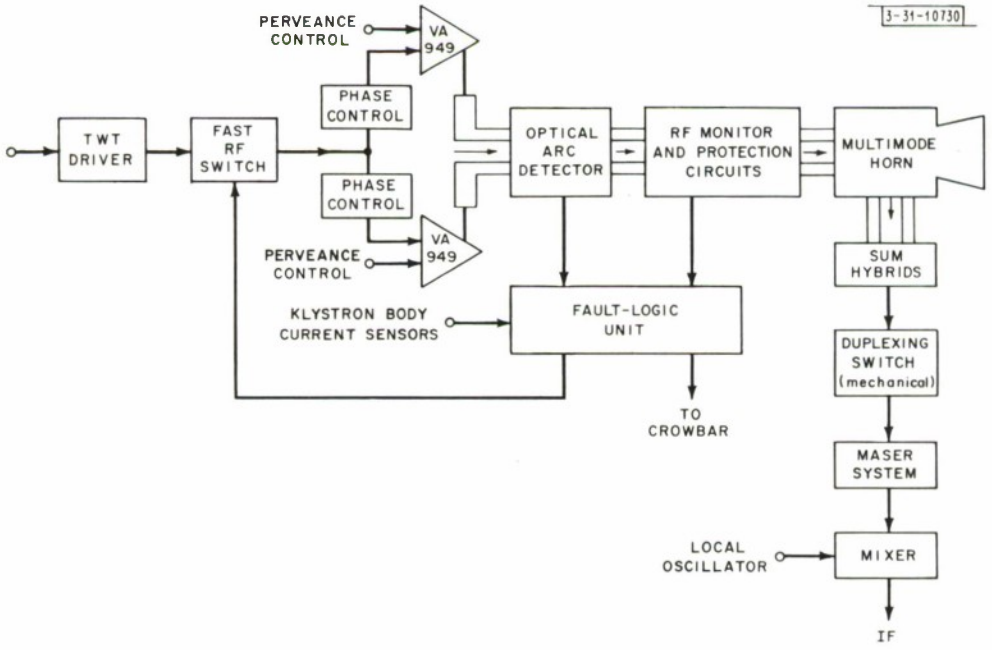

Fig. 2. Planetary radar microwave system.

experiments and as a passive radiometer. The special provisions for moon studies consist of providing short pulse capability plus polarization diversity.

The transmitter consists of a pair of VA-949AM, 250 kW, CW klystrons driven by a signal derived from a very stable source which controls all frequencies and timing operations at the Haystack station. The stable signal is multiplied to X-band and used to phase lock a CW klystron from which the drive signal, local oscillator signals, and certain test signals are derived by means of a frequency translation scheme. The output of the VA-949 klystron is carried in a four-waveguide transmission system to the multimode tracking horn which radiates the 500-kW signal into the Cassegrainian antenna system. The antenna, whose tracking feature is not actually used, is computer pointed for all experiments.

The radiated signal is right-hand circularly polarized. The return signal, which is left-hand polarized, is received at a set of four terminals which are isolated from the high power transmission system. It is then summed in hybrids and transmitted to the main receiver through switching circuits which further isolate the maser receiver from the high power line during the transmitting interval. Figure 1 is a simplified diagram of the radar and Fig. 2 a diagram of the microwave system.

Three important functions must be carried out in order to ensure proper operation and control of the RF system:

(a) Balancing of the klystron outputs

(b) Status monitoring of all critical parameters

(c) Protection of the equipment from damage due to some catastrophic event such as an arc in the waveguide.

The balancing of the system is accomplished by means of a phase control in the klystron drive circuits and the adjustment of the voltage on a control electrode in the klystron gun which has the effect of varying the perveance of the tube, thereby varying the amplitude of the RF output. The phase and amplitude equality is indicated by the balance of a microwave bridge which samples the waves in the output transmission lines. These same circuits, employing folded magic tee hybrids, also provide information on the total output power and provide signals to indicate sudden changes in the relative amplitudes, phases, or power levels in the four transmission lines which might be indicative of a major fault in the system.

If a CW arc develops in the system, and is not extinguished in a very short time (a few microseconds), the RF equipment, particularly the high power amplifier tubes, might be severely, probably irrepairably, damaged. The microwave monitor bridges will indicate some such faults. In addition, reverse power couplers have been placed near the tube output connectors and optical detectors have been incorporated which will detect any visible light near the tube windows. These fault detectors generate fast turn-off signals which will cause removal of the RF drive from the klystrons in a time of the order of a microsecond.

III. HIGH POWER RF AMPLIFIER

A. Description

The high power microwave system employs four parallel waveguide transmission lines. There were several reasons for choosing this particular configuration.

(1) A high confidence level had been built up around the 100 kW operation with the VA-879 transmitter. A four-waveguide 500-kW system would only provide a 1-dB increase in power level in the transmission lines.

TABLE I

CHARACTERISTICS OF VA-949AM KLYSTRON AMPLIFIERS

Operoting Chorocteristics (anticipated values)	250-kW CW Output	500-kW Pulse Output
Beom voltoge	52 kV	66 kV
Beam current	10 A	15 A
Heoter power (max)	150 wotts	150 watts
Heater voltoge	15 V	15 V
Heoter current	10 A	10 A
Collector caolant flaw (min)	80 gpm	80 gpm
Collectar pressure drap (max)	100 psi	100 psi
Body coalant flow (min)	15 gpm	15 gpm
Body pressure drop (max)	100 psi	100 psi
Caolont outlet temperature (max)	165°F	165°F
Coolant inlet temperature (mox)	120°F	120°F
Control electrode voltoge	Tied ta cothode	
Voltage far cut-aff conditians under pulse aperatian	−6.5 kV	−8.5 kV
Other Chorocteristics		
Electromagnet Requirements		
Voltage	300 valts max	
Current	10 omps mox	
Flaw	5 gpm	
Pressure	100 psi	
Weight af tube and magnet	525 lb	
Control electrode capacity	~100 pF	

(2) There were reasons to doubt that existing vacuum window designs would be trouble free at the 250-kW level. Unresolved problems existed with respect to window failures in the 100-kW VA-879 klystrons. For this reason, a two-window 250-kW tube seemed desirable.

(3) The multimode horn already in use in the Haystack antenna required four waveguide inputs.

A tracking multimode feed such as had been designed for the 100-kW system would not be needed for the planetary radar application, since all pointing would be done by the computer. However, the very efficient design was attractive and compatible with the four waveguide system which would be required to overcome an anticipated window problem in the high power klystron. There was also the problem of the circulators which would be required for moon mapping studies. These moon studies would be conducted using short pulses so that the average power would be low. However, there appeared to be no practical way to employ the circulators in the moon mapping mode and then to switch them out when operating in the CW planetary radar mode. This required that the circulators be installed permanently. The four-waveguide configuration was therefore compatible with all operational requirements and afforded a degree of conservatism which was expected to pay off in trouble free operation. The use of this configuration also reduced the power density to the point where waveguide pressurization was not necessary to avoid voltage breakdown. Only a small overpressure of dry nitrogen would be required to keep the system clean. As a result, the design of the horn radome was trivial, but it could have been difficult if pressurization had been required.

Two VA-949AM klystron amplifiers in parallel operation are the principal active elements in the planetary radar transmitter. These tubes were designed and constructed by Varian Associates specifically for this application and can be considered a direct development from the 100 kW VA-879 klystron employed in the earlier Radar/Communications (R/C) transmitter. Table I lists the important characteristics of the VA-949AM.

At the time the VA-949AM was procured, Eimac was developing an experimental klystron with the goal of achieving 1 MW CW at X-band. A power output of 500 kW was actually achieved for a short period. This achievement was very significant and it was attractive to consider a single-tube 500-kW transmitter. There were a number of factors against this, however.

(1) The Eimac tube was very large and heavy.

(2) The voltage required to achieve the 500 kW was beyond the capability of the Haystack power supply.

(3) The tube did not incorporate a modulating electrode which would be required for short pulse operation (moon studies).

A re-engineering of the tube could have removed some of the objections, i.e., the perveance could be increased and a collector designed for 500-kW operation which would reduce the weight considerably. However, even with these changes which would have been more costly than the Varian proposal, the size and weight of the Eimac tube would make its incorporation into the Haystack antenna system difficult.

As a five-cavity klystron power amplifier, the VA-949AM, Fig. 3, is unique only in the design of the electron gun which allows easy modulation of the electron beam. This gun configuration (Fig. 4) had previously been developed and successfully applied to lower power, i.e., 5 to 25 kW, CW tubes. Considerable engineering was required to adapt this type of gun to the 50 to 70 kV range required of the VA-949 and to this end a beam test vehicle (BTV) was constructed. This device contained all the necessary klystron components except the RF interaction section which was replaced by a continuous drift tube. Laboratory operation of the BTV allowed an

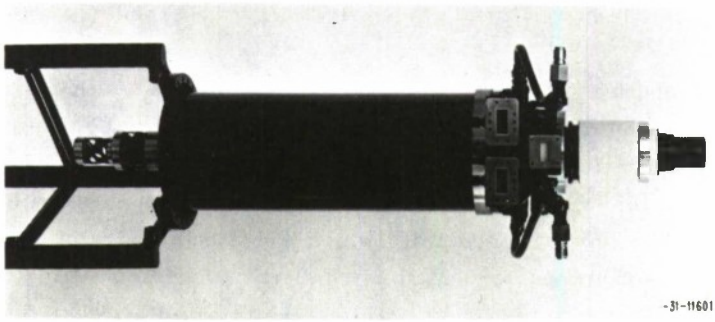

Fig. 3. Klystron VA-949AM.

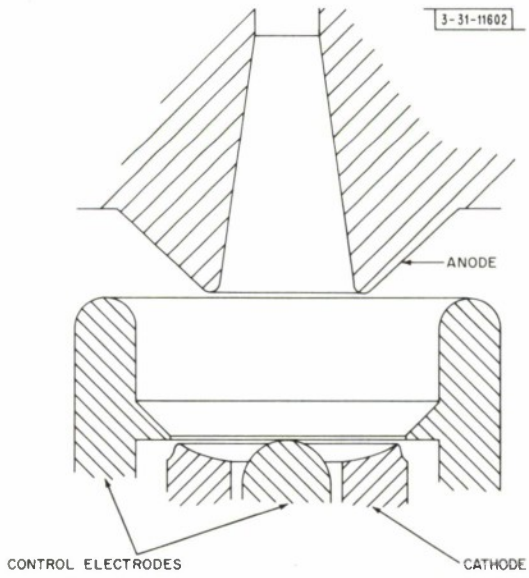

Fig. 4. Typical high-μ gun of type used in VA-949AM.

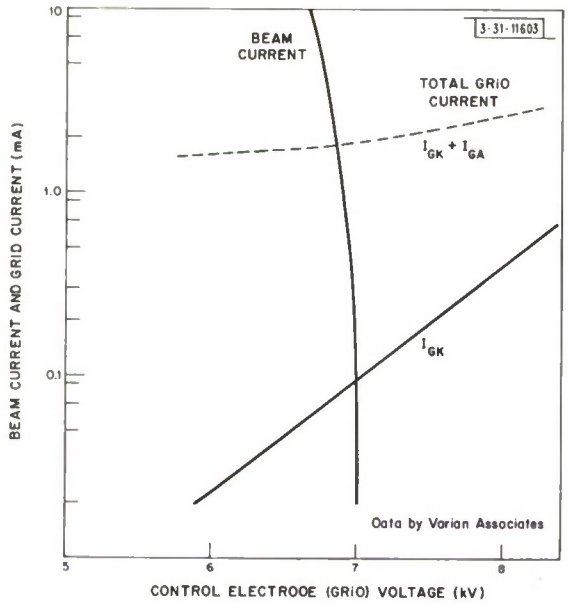

Fig. 5. Typical VA-949AM near cut-off beam performance at 55-kV beam voltage.

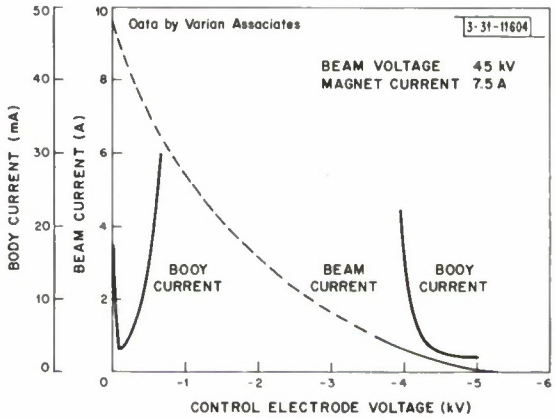

Fig. 6. Typical behavior of VA-949AM beam current and body current as a function of control electrode bias.

evaluation of the collector design and also provided a means of experimenting with gun design. Figures 5, 6, and 7 show the gun characteristics achieved in this experimental program.

While the gun characteristics achieved in the VA-949AM were not quite as good as had been achieved in lower power tubes using smaller cathodes, the incorporation of the high-μ control electrode was successful and made possible a small, lightweight, short pulse beam modulator (beam control unit) which was essential for the lunar studies and also provided a means for efficiently matching the RF output amplitudes of a pair of klystrons.

Typical performance of the VA-949AM is shown in Fig. 8.

B. Window Problem

When the earlier 100-kW transmitter using VA-879 klystrons was being designed, the best information from klystron manufacturers indicated that at the 100-kW CW level the most likely cause of window failure would be an RF arc moving against the vacuum window. In order to protect the klystrons from waveguide arcs, an arc detector using solid state sensors was designed which was capable of detecting arcs that could be sustained at RF power levels of less than 100 W. Nonetheless, there were three window failures at an RF level of approximately 80 kW CW which could not be attributed to waveguide arcs. This experience led to a survey of the microwave window "state of the art" and to some experiments at Lincoln Laboratory.

There had been earlier problems of window failure in microwave tubes and a number of studies were under way. As a matter of fact, a great deal of information was already available and in retrospect one wonders why these problems were not better understood in the tube industry than they appear to have been. The reason seems to have been that workers approached the problem from different points of view and with the feeling that theirs was the correct one. This, coupled with a number of competing failure mechanisms to choose from, resulted in an inadequate appreciation of the real problem.

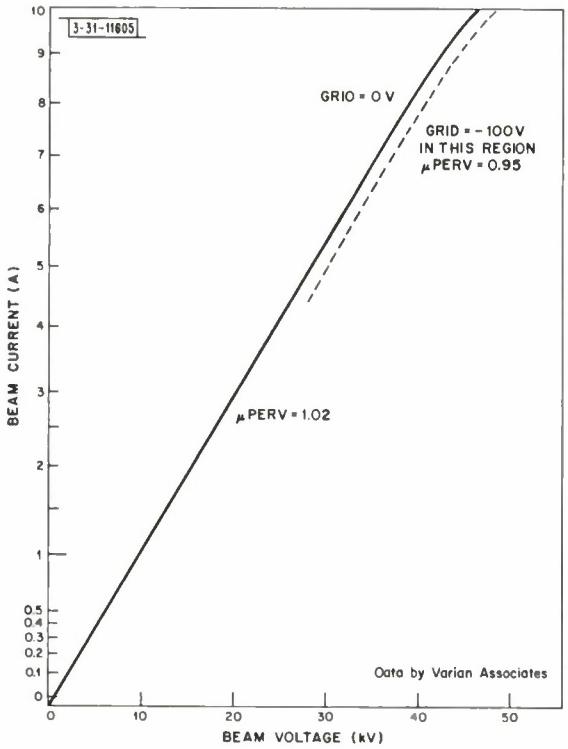

Fig. 7. Typical behavior of VA-949AM beam.

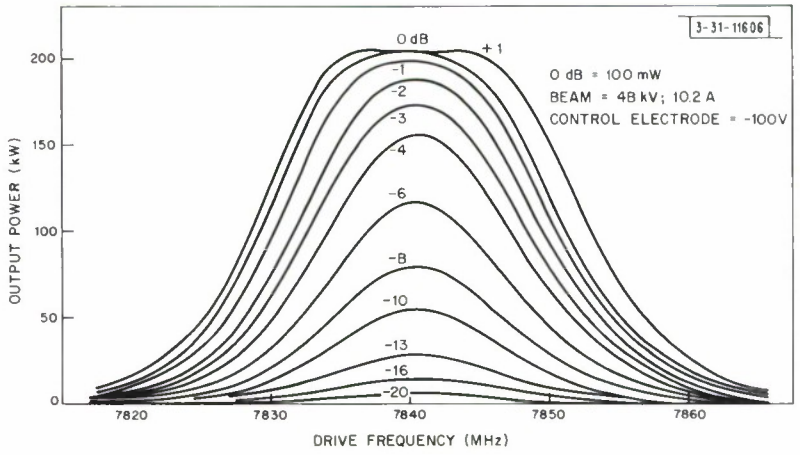

Fig. 8. Typical VA-949AM output characteristics for various levels of drive.

The principal window failure mechanisms are:

(1) Internal failure of the dielectric either by exceeding the dielectric strength or through generation of plasma in voids in the dielectric.

(2) Bombardment of the dielectric by high energy electrons which produce punctures through the dielectric from the vacuum side to the air side.

(3) Mechanical failure from shock waves generated by an RF breakdown in the transmission system.

(4) Window heating by (a) electron bombardment from the multipactor on the vacuum side of the window, (b) losses in the window dielectric, and (c) an RF arc coming against the external surface of the vacuum window.

Internal failure of the dielectric has not been experienced with CW tubes, but has been extensively studied at Stanford University because this type of failure has been an important one with the high peak power klystrons used in their accelerator program.[5,6]

Bombardment of the dielectric surfaces by high energy electrons has been an important factor in failures in older tubes, but all modern high voltage klystrons are designed so that the windows are shielded from high energy electrons escaping from the beam.

For some time it has been questioned whether RF discharge generated shock waves were responsible for window damage in microwave tubes. Lincoln Laboratory experiments[7] indicate that X-band size thin windows should survive shock waves generated by RF arcs up to a power level of about 220 kW and that thick windows of the type used by Varian in the VA-879 and VA-949 klystrons should not be subject to this type of fracture below the megawatt level.

Thermal cracking of RF output windows is the principal window failure mechanism in CW tubes. The problem reduces to that of failure due to the combined heat load from the multipactor discharge on the vacuum side of the window and from the dielectric losses within the window material itself. Considerable work has been done on these problems by investigators at Varian, Eimac,[8] RCA,[9] and Lincoln Laboratory.[10,11] Despite the quantity and quality of the work done prior to mid-1965, when the VA-879 window problem was encountered, there appeared at that time to be considerable disagreement among the various authorities in the field. This led to the Lincoln Laboratory experiments.

C. E. Muehe[11] has shown that the power level at which a half-wavelength rectangular window will break when the heat input is from the dielectric losses alone may be expressed as:

$$P_T = \frac{4a^2\epsilon' - \lambda^2}{2a^2\epsilon' - \lambda^2 + 2a^2} \frac{k\sigma_T}{\alpha E \epsilon''} \frac{3}{8\pi} \frac{\lambda^2}{\lambda_g} \left(11.4 \frac{b}{a} + \frac{8a}{b}\right)$$

where

σ_T = tensile strength

α = temperature coefficient of expansion

E = Young's modulus

k = thermal conductivity

ϵ' = real part of dielectric constant

ϵ'' = imaginary part of dielectric constant

a and b are waveguide dimensions in centimeters

The material constants used in the calculation of the thermal failure point are shown in Table II. The coefficients α, σ_T, and E used were those quoted for the maximum temperature rise plus the assumed ambient temperature of 40°C. Constants used in this table are an average of values quoted by various manufacturers.

TABLE II

MATERIAL CONSTANTS* FOR VARIOUS WINDOW DIELECTRICS

Constant	99.5 Percent Alumina	Lucalax or Synthetic Sapphire	Beryllia	Fused Quartz
σ_T (psi)	25×10^3	55×10^3	21×10^3	15.5×10^3
α ($°C^{-1}$)	7×10^{-6}	6×10^{-6}	6×10^{-6}	0.55×10^{-6}
E (psi)	5×10^7	5×10^7	5×10^7	1.07×10^7
K (watt/cm °C)	0.72	0.42	2.0	0.017
ϵ'	9	9.4	6.0	3.9
ϵ''	0.002	0.0006	0.0027	0.0004

* Constants are an average of values quoted by several manufacturers.

TABLE III

CALCULATED FAILURE LEVELS DUE TO DIELECTRIC LOSSES AT 7.75 GHz FOR WR-137 HALF-WAVELENGTH BLOCK WINDOWS

Material	Average Power (kW)	Temperature Rise af Center Over Edge (°C)
99.5 percent alumina	147	107
Lucalax and synthetic sapphire	1950	275
Beryllia	750	105
Fused quartz	151	3950 (400)*

* Quartz will melt before it cracks. For all calculations, a value af 400°C was used, because the lass tangent starts ta increase rapidly at this temperature.

Table III shows the results of calculations made for half-wavelength rectangular windows in WR-137 waveguide at a frequency of 7.75 GHz. For 99.5 percent alumina, the average breakage level is 147 kW. The spread is approximately 125 to 175 kW depending on the particular values of the material constants chosen from the available data.

Assuming the windows used in the VA-879 klystrons which fractured at approximately 80 kW were of high quality alumina, the conclusion was that there must be a heat source contributing to window failures besides the heating due to dielectric losses.

A multipactor (electron resonance) phenomena had been suspected for some time as the principal cause of window failures in klystrons in the Stanford accelerator. Preist of Eimac showed that a single surface multipactor[8] was possible, and developed an expression which predicted the threshold for multipactor on the vacuum side of a dielectric window.

$$V_e = 2 \frac{e}{m} \left(\frac{E_p}{\omega}\right)^2$$

where V_e is the electron velocity expressed in electron volts, e/m is the charge to mass ratio of an electron = 1.76×10^{11}, and E_p is the peak electric field parallel to the window surface. For the case of a half-wavelength window, the transmission line will be matched and the power passing through the window will be

$$P_T = \frac{1}{2} \frac{E_p^2 h^2}{377(\lambda_g/\lambda)}$$

where $E_p h$ is the voltage at the center of the waveguide.

Preist found that for windows which had been subjected to repeated or extended bake-out, the maximum electron velocity of window generated electrons was 40 to 80 electron volts. Using these numbers and assuming WR-137 waveguide at 7.75 GHz the critical power level is found to lie between 74.2 and 148.4 kW. Preist states that in some cases where the bake-out was of short duration, the power level at which excess heating occurred corresponded to maximum electron velocities of only a few volts. This was attributed to contaminants on the window surface which were subsequently removed by further processing. The lower limit found by Preist for "clean" alumina was about the level at which VA-879 failures had been experienced. The upper limit of nearly 150 kW was the power level at which Varian claimed to have successfully operated alumina block windows in "windowtrons" in a traveling wave resonator.

In order to obtain further data some "windowtrons," Fig. 9, were procured from Varian. It was also intended to install these at the output of the VA-879AM to protect the windows from shock waves induced by RF breakdown. It was later established by R. Weigand[7] that shock wave breakage of thick windows of the type used in the VA-879 and VA-949AM klystrons was very unlikely at power levels below the megawatt range. For this reason windowtrons were not incorporated in

Fig. 9. "Windowtron."

the 500-kW Haystack transmitter although one was installed for a period of time in the 100-kW system.

High power laboratory windowtron tests, using a resonant ring, employed a Varian photo multiplier arc detector which was installed so as to have the window receiving the incident RF wave in its field of view. The photo multiplier type of arc detector is more than an order of magnitude more sensitive than the solid state detectors initially employed with the VA-879 100-kW transmitter.

The performance of the "windowtrons" was quite variable. One particularly interesting series of tests contributed a great deal to the better understanding of the window problem. In this test, a windowtron was installed in the ring resonator and the power slowly increased. At the 80-kW level the arc detector, observing the incident window, shut down the transmitter. When power was turned on again, shut-down occurred at about 6 kW. Observations were then made with the unaided eye looking at the "windowtron" window through a small hole in the waveguide. The arc detector was disabled and power turned on and off manually. Each time the RF power was turned on a faint glow was seen through the ceramic window. No light could be seen at the other "windowtron" window, even with the arc detector, indicating that the discharge responsible for the light was restricted to the near vicinity of the incident power window. After several hours of turning off and then restoring the power, the window "cleaned up" and was eventually broken at 140 kW CW. The break occurred without any indication of light coming from inside the "windowtron" prior to the actual break. At that time all sensors, i. e., vac ion monitor, reflected power monitor, and arc detector, indicated a fault. The failure occurred at a power level very close to that predicted for heating due to dielectric losses and is therefore a confirmation of the validity of that calculation. The accuracy of these predictions was further demonstrated later at Eimac where a beryllium oxide window failed at about 700 kW CW, close to the 750-kW prediction.

The experience in the Lincoln high power RF laboratory demonstrated that both RF heating and multipactor bombardment are factors in window failure, the latter being unpredictable. The fact that a window has been "cleaned" by extended or repeated processing does not seem to guarantee that it cannot somehow become contaminated during normal operation of a tube. It is reasoned that this occurs as a result of a "gas burst" near the window which ejects material on the window, thereby lowering the level at which secondary emission can occur. This may be associated with seal problems which have long been considered in the tube industry to be related to the window failure problem. If this contamination is not too great, it can be cleaned up by a low intensity multipactor. This has been done with several klystrons, both the 100-kW VA-879 and the 250-kW VA-949, which have exhibited a tendency to develop multipactor when first installed in the transmitter.

As a result of the high power laboratory experience, all solid state arc detectors were replaced by detectors similar to the Varian commercial unit which employs a vacuum tube photomultiplier. These are incorporated in the transmitter control system in such a way that the RF drive on the klystrons will be turned off when the photomultiplier current exceeds a set threshold. It has been the practice in breaking in new tubes to run them at a power level which produces a photomultiplier output just below the threshold. This allows a small amount of multipactor which tends to clean up the window after a period of operation.

The specifications for the VA-949AM 250-kW CW klystron were written to reflect conservatism in the window design. The output power is divided within the vacuum envelope of the tube

and the power removed through two windows. This should be within the safe operating limits of alumina windows, however B_eO windows were specified in order to provide a further margin of safety. It later developed that B_eO windows are apparently less prone to support multipactor than are alumina windows. The reason for this is not understood at the present time.

As a result of consideration given to all aspects of window failure and the conservatism in the design approach taken with the VA-949AM, there has not been a single klystron failure in the Planetary Radar attributable to the RF window.

IV. HIGH POWER TRANSMISSION SYSTEM

A. System Description

The four high power RF output ports on the two VA-949 klystrons are fed through four Raytheon PXH26 circulators into the four input ports of the multimode feed horn. Sensors associated with the control, monitoring and protection of the high power RF amplifier are incorporated as a part of this transmission system. Figure 10 shows the details of the transmission system associated with one of the klystrons and the way in which the monitor circuits are connected in order to provide information on the balance between the two klystrons, and to allow measurement of the total transmitted power.

To achieve a satisfactory radiation pattern from the antenna, it is necessary that the four input ports be excited with equal amplitude to within 1.6 dB and equal phase to within 11.5°. One of the functions of the monitoring network is to sample the forward RF power in each of the four channels, and to compare these samples in phase and amplitude in a waveguide hybrid network. The four transmission lines from the klystrons to the feed horn are provided with directional couplers which sample the forward going wave and are connected to bridge circuits composed of folded magic tees. These couplers are constructed in matched pairs which were very carefully adjusted by the manufacturer to have identical coupling. The folded magic tee used in the bridge circuit is an integral part of the coupler pair. It is symmetrically located so that waves transmitted through the system which are equal in amplitude and phase with respect to the input flanges of the assembly cause a null of −25 dB or better to be achieved at the difference port of the folded tee. This port is labeled LINE UNBALANCE in Fig. 10.

The two bridges associated with the upper and lower klystron transmission lines are connected to a third bridge in a symmetrical fashion as shown in Fig. 10, allowing a similar comparison between the transmission systems of the two klystrons. Any imbalance between transmission channels appears as an error signal at the difference port of one or more hybrids. These error signals are available to the operator at the control console. Since the klystrons are normally operated with the RF drive at the saturation level, equalization of the power output of the two tubes is best obtained by adjustment of the grid-cathode voltages, i.e., adjustment of the perveance of the klystron gun. The adjustment of the relative phase of the two tubes is accomplished by means of phase shifters in the RF drive channels. It is necessary that the whole microwave system be symmetrical. Because of tolerance problems associated with waveguide systems, it is necessary to provide line length adjustments to equalize the electrical lengths of the four transmission lines. This is done in the following manner:

(1) The complete microwave system is assembled up to and including the circular polarizers in the horn feed. A short-circuiting plate is bolted over the four-pipe aperture at the end of the circular polarizer. A special four-way power divider which has been carefully constructed is connected to the flanges normally bolted to the klystrons. Detectors are

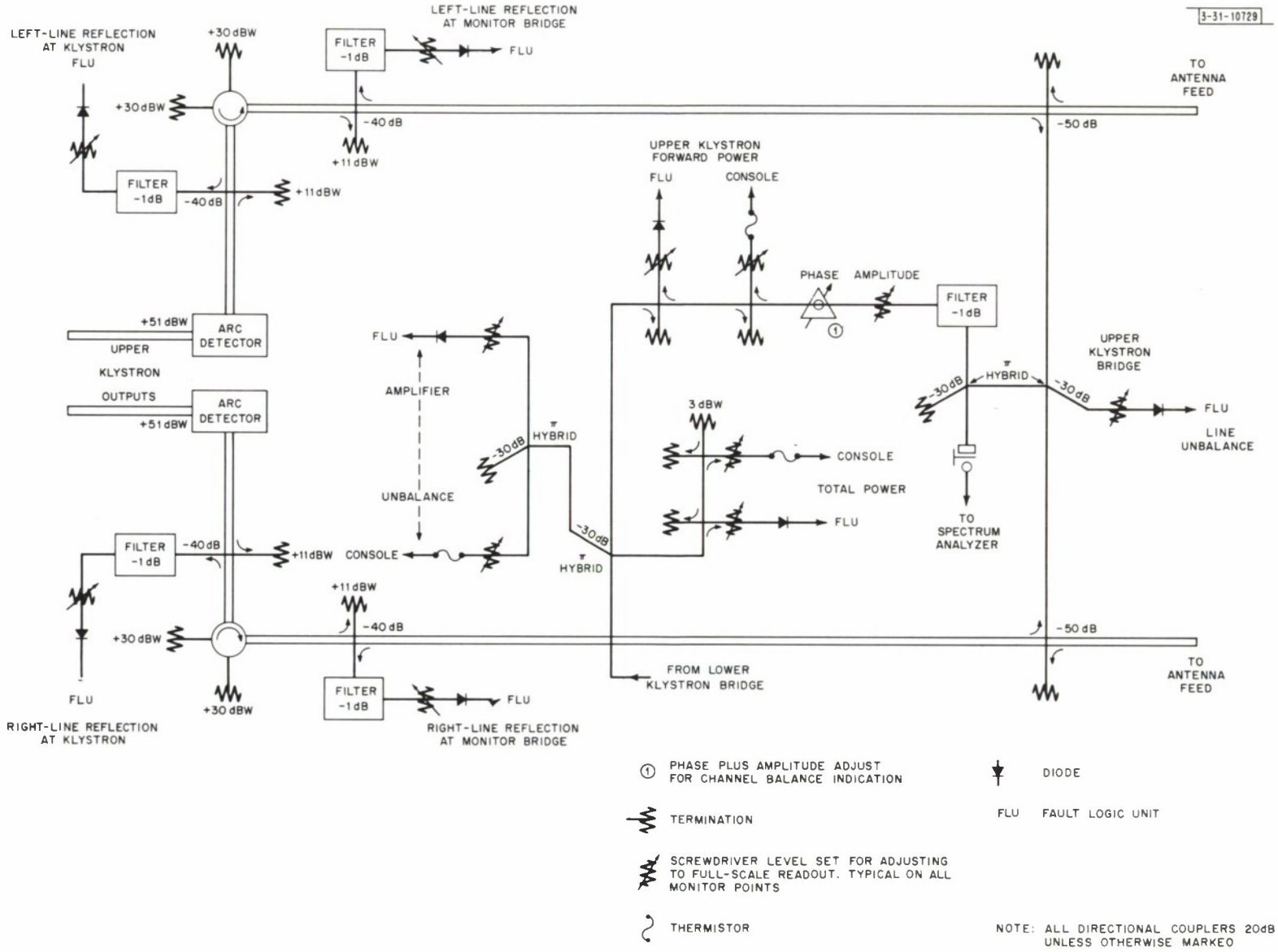

Fig. 10. Transmission system associated with one of VA-949AM klystrons.

connected to the difference ports in the monopulse circuits and in the monitor bridge circuits.

(2) The waveguide is shimmed between the four-way power divider and the monitor couplers to produce nulls at the detectors on the three difference arms of the bridge circuits. This assures that the signals are in phase at the reference flanges of the coupler assemblies.

(3) It is necessary that the transmitted signals be in phase at the horn. If they are in phase, deep nulls will be obtained at detectors placed on the monopulse difference ports when the feed is short circuited. Shims are placed in the transmission lines between the monitor couplers and the feed assembly to achieve these deep nulls.

(4) After this alignment has been achieved, the shims are removed and measured, and copper gaskets of the proper thickness are constructed for use in the high power system.

When the actual klystron amplifiers are installed and operated, the perveance adjustments and the input phase adjustments are used to obtain a good null at the amplifier unbalance detector, Fig. 11. It was found that the tolerances on the klystron windows and output sections were such that it was sometimes necessary, when changing tubes, to re-shim the lines connected to a single tube in order to achieve good nulls at the unbalance detectors associated with that pair of transmission lines.

In the initial planning of the 500-kW transmitter, it was envisioned that a phase control loop might be required to maintain phase balance at the output of the two tubes. It was later reasoned that this should not be necessary if the tubes met the stability specifications. This was subsequently demonstrated to be the case for tubes which meet specifications. No phase correction loop is used in this system and none is contemplated.

B. High Power Transmission

Two problems presented by the transmission of large amounts of power in small waveguides are (1) voltage breakdown in the dielectric gas filling the waveguide, and (2) heating of the waveguide because of the finite conductivity of the waveguide walls.

1. Voltage Breakdown in Waveguide Dielectric

The breakdown power in watts for a smooth rectangular waveguide filled with dry air at atmospheric pressure and above is

$$P_B = \frac{E_m^2}{4\zeta} ab \left(p \frac{T_o}{T}\right)^2 \frac{\lambda}{\lambda_g}$$

where p is in atmospheres, T is the absolute temperature of the air, $T_o = 290°K$, a and b are the waveguide dimensions in centimeters, $\zeta = 376.8$ ohms, and E_m is the dielectric strength of the gas at a pressure of one atmosphere in volts/cm.

At high frequencies the primary ionization due to electron motion is the only mechanism which controls breakdown.[12] The presence of electron sources in the transmission system, such as (a) series arcing at poorly made joints, and (b) particles of foreign material which are heated to incandescence by the microwave field (dust for example), can play a large role in determining the power handling capability of the waveguide. In a CW system the presence of one of these ionization sources will surely result in breakdown. In the case of high peak power pulsed systems, the pulse may be short enough that the breakdown does not always occur even though series arcing may be present or incandescent dust particles may be observed drifting across the waveguide.

When CW systems are first turned on, breakdown may be experienced until dust particles are burned out.

Even though considerable care was taken in the cleaning and assembly of the Haystack components, breakdown problems sometimes began to appear after several months of operation. Disassembly of the transmission system revealed unexplainable small black specks in the waveguide. Careful chemical cleaning, washing and drying removed these deposits and the reassembled system functioned without trouble for another considerable length of time. The source of the contaminant is not known. However, in high power laboratory experiments using fabricated components, difficulty was experienced on several occasions when the RF system broke down at a power level somewhat lower than expected. After this initial breakdown the highest power level that could be reached before another breakdown occurred was sometimes as much as an order of magnitude lower than that initially achieved.

Close examination of the RF system revealed the presence of corrosive fluxes which had apparently been driven out of voids in the fabricated components by the RF heating of the waveguide. Careful cleaning would restore the system to its original capability, but it was never possible to rework the faulty component so that its performanee was brought up to the expected value. When this sort of failure occurred, the corrosive materials were driven throughout the microwave system so that the whole system required cleaning, not just the component with the flaw. Because of this type of experience, high power components were purchased only from a source which had proven its ability to produce fabrications that did not contain entrapped corrosive material. In addition, every component was high-power tested well beyond its requirements before installation in the Haystack high power system.

Two standard waveguide sizes are employed in the transmission and monitoring system. WR-112 is normally used in the 7.7 to 8.0 GHz band because a large number of components are available in this size. However, the larger size WR-137, can be used as high as 8.2 GHz and was chosen for the high power transmission line principally to ensure as large a margin of safety as possible against voltage breakdown. The smaller WR-112 is used extensively in the receiving circuits and in the monitoring and protection system.

The calculated breakdown power for WR-137 waveguide at one atmosphere of dry air is 2.75 MW at a temperature of 290°K. It has been found, experimentally, that if proper flanging and gasketing techniques are used, and care is given to component fabrication, reliable performance can be achieved at power levels considerably in excess of the 125-kW CW level required in the planetary radar. Under these circumstances it is not necessary to operate the waveguide system at higher than atmospheric pressure. In laboratory resonant ring tests, unpressurized breakdown occurred at 933 kW at a cross-guide coupler.

2. Heating of Waveguide

The heating of a waveguide is directly related to its attenuation which may be expressed as

$$\alpha = 1.58 \frac{\lambda}{2a} \frac{(a/b) + 2(\lambda/2a)^2}{\sqrt{1 - (\lambda/2a)^2}} \frac{1}{(\lambda^3 \sigma)^{1/2}}$$

All dimensions are in meters; α in dB/meter, σ = conductivity in mhos/meter, and a and b are the waveguide inside cross section dimensions. This expression gives, for pure copper waveguide, 0.079 dB/meter for WR-112 and 0.051 dB/meter for WR-137 at 7840 MHz. OFHC

copper, whose conductivity is essentially that of pure copper, was used as a waveguide material throughout the Haystack system. In a high average power system such as the Planetary Radar, it is necessary to provide cooling for the waveguide in order to (a) avoid a personnel hazard, (b) prevent thermal damage to electronic devices associated with the transmission system, and (c) prevent a reduction of the voltage breakdown level. The seriousness of this problem may be seen when it is realized that the temperature rise above ambient for a horizontal run of WR-137 OFHC copper waveguide cooled only by natural convection and radiation would be about 300°C when transmitting an average power of 50 kW.

The most effective cooling method is to remove the heat in a fluid such as water so that it may be disposed of without seriously affecting the temperature of the immediate surroundings. A satisfactory method is to secure 1/4-inch copper tubing to two opposing sides of the waveguide and to flow water through at the rate of about 1 gallon per minute.

The thermal contact with the waveguide can be made with either soft solder or with a metal-bearing epoxy, some of which have heat conducting properties equal to or better than lead-tin solder. In any case, the tubing should be fastened to the waveguide, particularly at its ends where stresses will be applied during attachment to the water system, by some means which affords greater strength than lead solder or epoxy. Silver soldering a spot near the ends of the cooling tubing is satisfactory.

3. Waveguide Breakdown Due to Flange Joints

High power laboratory experience has shown that the flanged joint represents the greatest uncertainty in a transmission system. It is the primary cause of waveguide breakdown where care has been taken to choose components whose design reflects consideration of the voltage breakdown problem. There are two principal causes of breakdown:

(a) The flanges do not make a good metal-to-metal contact. The resulting series arcing provides a source of ionization which precipitates breakdown across the waveguide.

(b) The joint is misaligned, the mating waveguides at the joint are not of exactly the same size, or the opening at the joint has been deformed presenting a sharp edge to the electric field.

A waveguide gasket has frequently been used to help overcome the flange joint problem. However, commercially available gaskets are designed primarily to provide pressurization and are poorly designed, particularly in the case of the smaller waveguide sizes, to satisfy the high power RF contact requirements. High power laboratory experience has led to the development of a flange, gasket, and assembly procedure which produces results greatly superior to those of anything available commercially. This has been done in a way which is completely compatible with Electronic Industries Association (EIA) standards. In this scheme, a special soft copper gasket is clamped between two stainless steel CPRF (connector, pressurizable, rectangular, flat) flanges which have been lapped to be as flat as possible. After the waveguide and gasket openings have been accurately sized, the assembly is made with care to insure accurate alignment and uniform pressure distribution around the waveguide periphery.

The ideal flanged joint will appear to the microwave field as though there were no joint there at all. In order to approach this ideal as closely as possible, the following steps are taken:

(a) The type of flange used is that in which the copper waveguide goes all the way through. Socket type stainless steel flanges are not suitable for high power applications.

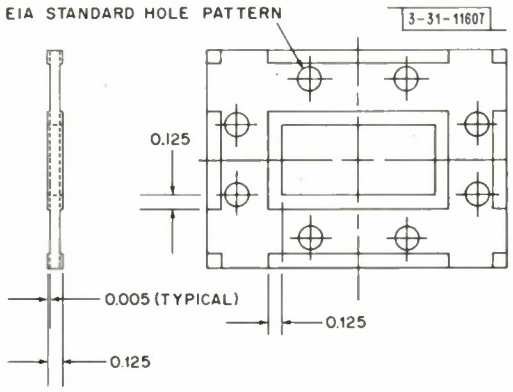

Fig. 11. Gasket for use with CPRF 137 flange.

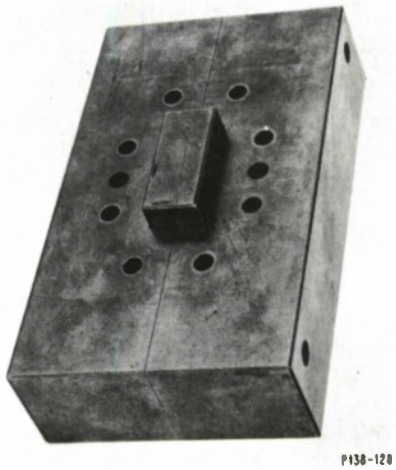

Fig. 12. Drill jig.

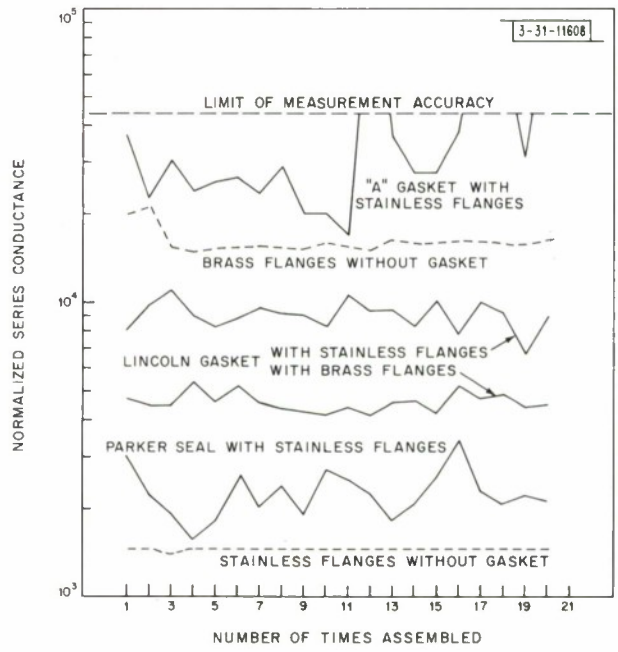

Fig. 13. Measured flanged joint conductivity at 7.05 GHz in WR-112 waveguide.

(b) The waveguide opening and the gasket opening are sized to the maximum waveguide dimension with a sizing plug which is a part of the flange drill jig.

(c) The holes are precision drilled so that dowel pins are a good fit.

(d) After the sizing operation (and drilling if the holes are not already there) all mating surfaces are lightly lapped to insure flatness.

(e) The assembly is made by aligning the joint using dowel pins in two opposing sets of holes while the remaining holes are bolted up using precision high strength bolts. The dowel pins are then removed and bolts inserted. Bolts are drawn up using a torque wrench to 50 inch-lb for WR-112 line, and 60 inch-lb for WR-137 line.

The force required to draw the joint together so that the copper gasket is slightly crushed and in good contact with the waveguide is sufficient to seriously disturb brass flanges, even if they are extra heavy. Stainless steel flanges have proven to be of sufficient strength and can be bolted many times without fear of distortion. The CPR configuration is the only standard flange that is acceptable for high power systems. The bolt holes in the old style square flange are too widely spaced and too far from the waveguide wall to provide adequate gasket pressure. Figures 11 and 12 show the gasket and drill jig designed at Lincoln Laboratory.

The Lincoln Laboratory gasket does not incorporate a pressurization seal at this time, although one could easily be incorporated. The Haystack system is unpressurized except for about 1/4 lb nitrogen overpressure to keep the waveguide clean internally. The plain gaskets provide a sufficiently tight seal to limit the leakage rate to a tolerable value. A seal is desirable, however, because there are many components in the Haystack transmitter which must be cooled by the distilled water system. Occasionally a water fitting develops a leak or a plastic pipe pulls out of a connector spraying considerable water on the waveguide assembly. This tends to seep down into the flange joints and has on a few occasions produced corrosion of the copper gasket and waveguide in the area where a metal to metal contact must be maintained. This has not yet been a serious problem, but a gasket incorporating a seal is under consideration for future use.

Stainless steel is very lossy compared to copper. In extremely high power systems it is prudent to insure that only copper is exposed to the RF field. Socket type flanges are, therefore, not acceptable because the flange material forms a short section of waveguide. In addition, the stainless steel is so hard that it cannot be properly sized to insure a smooth joint.

It has sometimes been the practice to butt two flanges together, thus eliminating the gasket where pressurization is not a problem. This works reasonably well using brass or aluminum flanges. However, it has been found that for stainless steel flanges, the machining and lapping process will remove copper faster than stainless steel, and as a result flange-to-flange joints, where through-type stainless flanges are used, will have a small gap between the ends of the copper waveguides. This can lead to series arcing in high power systems. The joint is also more lossy than would be obtained with a proper copper-to-copper contact (see Fig. 13).

Figure 14(a) shows the results of some high power tests of flanged joints when extreme care was used in the assembly. Both the gasket opening and the waveguide openings were sized each time the joint was assembled. The gasket orientation was not preserved, however. The curve marked "Lincoln Gasket" is for the gasket shown in Fig. 10. Gasket "A" was an experimental gasket in which the contact area at the waveguide opening had been reduced in order to apply a greater contact pressure. The result was that a very thin lip would turn down in the waveguide when pressure was applied. This could not be removed by sizing alone, but could be removed by a combination of sizing and lapping of all mating surfaces. In a practical system it is not convenient to lap all surfaces for each assembly so this design was not used.

TABLE IV

HIGH POWER TEST RESULTS*

Component	CW Power at Breakdown (kW)	Waveguide Size
H-plane hybrid (1)	170	WR-112
H-plane hybrid (1)	200	H arm WR-137 other ports WR-112
Short slot hybrid (2)	205	WR-137
E-plane hybrid (1)	155†	WR-112
OMT (2)	272†	WR-112
OMT plus polarizer (2)	257†	WR-112
Circulators (5) (1)	175† 200†	WR-137 WR-137
Window (B_eO) (1)	430†	WR-137
Rejection filter (1) (8.050 GHz)	175	WR-112

* Test frequency = 7.75 GHz

† Did not break down.

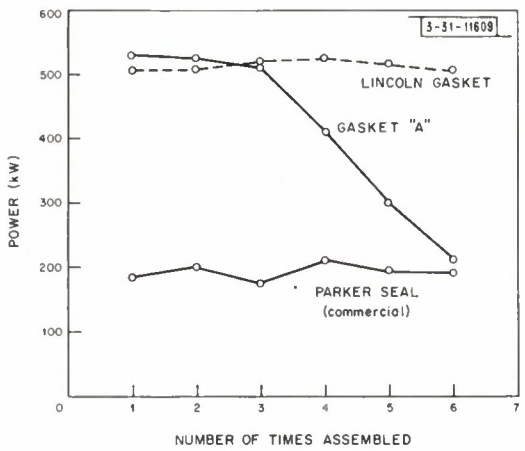

Fig. 14(a). Average breakdown power for several WR-112 gaskets precision sized and aligned for each assembly.

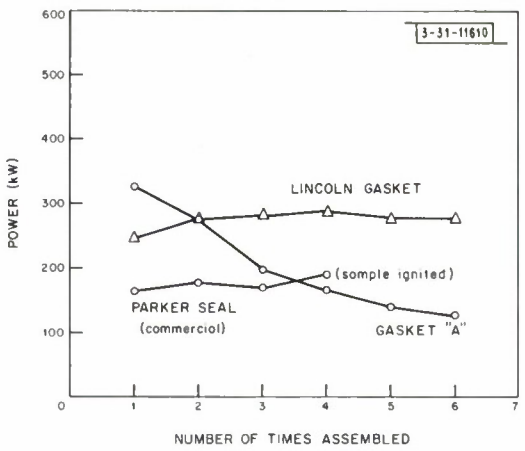

Fig. 14(b). Average breakdown power for several WR-112 gaskets that were not precision sized and aligned for each assembly.

Figure 14(b) shows essentially the same joint behavior when the sizing operation and the use of dowel pins for alignment are eliminated from the procedure. It should be mentioned that the gasket and waveguide openings were sized when the bolt holes were drilled. The Parker seal comes drilled but most of them, as received from the manufacturer, have had undersized waveguide openings. These were all brought up to the standard opening with the sizing plug.

Since this series of tests was conducted, the Lincoln gasket has been successfully used at Haystack. Some of the joints have been broken many times and the gaskets reused without any apparent degradation of the transmission system.

V. HIGH POWER COMPONENT DEVELOPMENT AND TESTING

A. Introduction

It is well known that practical CW waveguide transmission systems do not even closely approach the power handling limit calculated for smooth waveguide. So little data were available at the beginning of the Haystack program that it was necessary to evaluate the power handling capability of commercially available components as well as to develop those special devices required by the system. In order to establish practical limits of power handling capability, several individual items of the same type were tested whenever possible. These included directional couplers, bends, orthogonal mode transducers, quarter wave plates (circular polarizers), hybrids, ferrite circulators, filters, and flanged joints (see Table IV).

B. High Power Traveling Wave Resonator

The tests were carried out using a high power traveling wave resonator,[13] a well known technique. A traveling wave resonator, or resonant ring, consists of a closed loop of waveguide which is an integral number of guide wavelengths long. RF power is coupled into the ring by means of a directional coupler. If the coupling value is chosen so that all the available RF energy will be absorbed by the ring, the ring gain will be given by[14]

$$P_R/P_T = \left(\frac{1}{C_o}\right)^2 = \frac{1}{1 - T^2}$$

where P_R is the forward power in the ring, P_T is the forward power from the transmitter, C_o is the coupling factor, and T is the ring transmission factor. For this case, the gain in dB is equal to the magnitude of the coupling value in dB. If the ring is lossless (i.e., no energy can be dissipated in the ring), the gain would be approximately 6 dB greater than the coupling value, actually 5.8 dB when using a 10 dB coupler. The ring used in high power testing the components for the Haystack radar used a 10-dB directional coupler and had a power gain of 12 to 14 dB depending upon the loss of the component under test. Using a VA-849 klystron (nominal 25-kW output) as a power source, ring power levels of over 500 kW CW were obtained.

When breakdown occurs in a ring resonator, the voltage at the arc is reduced to the sustaining voltage of the arc and the ring is detuned by the reactance presented by the arc. As a result, the power dissipated in the arc is low, of the order of the transmitted power multiplied by the coupling value (typically −10 dB or less). This self limiting feature of a resonant ring minimizes arc damage when breakdown occurs. In addition, fast turn-off circuits are employed to turn off the RF source as a further safeguard in limiting component damage. The fast turn-off circuits are activated by signals from light sensing detectors and reverse power couplers which are so arranged that arc faults are detected as soon as they occur. Similar more sophisticated circuits are used in the Haystack microwave system to protect the high power klystrons and other components from serious damage.

Resonant rings in both WR-112 and WR-137 waveguide were employed in the Haystack program. They were assembled from a stock of carefully constructed components with special attention given to the quality of the flange joints. Coupling to the fixed tuned rings was accomplished with sidewall multi-hole couplers. Their lengths were made such that resonance was obtained reasonably close to the test frequency (7.75 GHz). Final adjustment was made by moving the test frequency within the pass-band of the klystron amplifier serving as the power source.

One of the most difficult problems in ring testing is to reduce the amplitude of the back coupled wave. This backward wave is produced by imperfections in the directional coupler and by reflections in the ring, usually those produced by the component under test. In almost all cases it was possible to reduce the back wave to −20 dB or lower by various techniques which are familiar to ring users. In the case where circulators are tested the back wave is automatically terminated so that the ring adjustment procedures are greatly simplified.

In high power component development, it is desirable to ascertain the point in the transmission system where breakdown occurs. The test circuits are customarily set up so that one can observe the component under test through a viewing port usually located in a waveguide bend. Even if the point where breakdown occurs is visible it is often difficult to accurately determine its position. Furthermore, if fast turn-off circuits triggered from an optical arc detector are used, the eye will not be able to see the breakdown. A scheme was suggested by Brown[15] which enables the arc to be located within about ±1 cm. In this scheme an oscilloscope is triggered from a reverse power detector or an optical arc detector when the arc occurs. A small microphone picks up sound waves generated by the arc. These are applied to the oscilloscope. The length of the sweep out to the point when acoustic signals begin to appear is a measure of the distance from the microphone to the arc.

The velocity of sound in air[16] at one atmosphere pressure,

$$v = 33{,}145 \sqrt{\frac{T}{273}} \text{ cm/sec}$$

where T is the absolute temperature, must be corrected for the viscosity of the air which tends to reduce the velocity when it is confined in a pipe:[17]

$$v_1 = v \left[1 - \frac{c}{2s} \sqrt{\frac{\mu}{2\omega\rho}} \right]$$

where c is the perimeter of the pipe and s the cross sectional area. μ/ρ is the kinetic viscosity constant equal to 1.75 cm^2/sec for air at 40°C and a pressure of one atmosphere. This correction reduces the velocity by 0.3 percent for WR-137 waveguide at a frequency of 70 kHz.

The presence of water vapor increases the velocity[18]

$$v_1 = \frac{v}{\sqrt{1 - 0.38 \, (P_1/P)}}$$

where P_1 is the partial pressure of water vapor and P the atmosphere pressure. A partial pressure of 1 mmHg of water vapor will increase the velocity of sound by 0.25 percent at a pressure of one atmosphere.

The RF discharge produced by waveguide breakdown heats the air and produces a shock wave. When the system is protected by fast turn-off switches the shock wave does not have time to grow, so the overpressure is extremely small and no correction is necessary. For 25 kW power level at 7.75 GHz the peak shock strength occurs about 300 μsec after the initiation of the discharge in the waveguide. The resulting overpressure is about 0.1 and appears to be proportional to the applied RF power. Fast turn-off circuits can remove the power in less than 5 μsec.

For microwave systems not protected by fast turn-off circuits, the velocity of the shock wave must be taken into consideration. The velocity of weak shock waves is given as[19]

$$v_1 = v \left(1 + \frac{\gamma + 1}{4\gamma} \frac{\Delta p}{p}\right)$$

where γ is the ratio of the specific heats of the gas ($\gamma \simeq 1.4$ for air) and $\Delta p/p$ is the relative overpressure.

This technique was employed in connection with some of the high power ring tests and appears to have possible applications in debugging high power transmission systems.

C. High Power Ferrite Circulators

The requirement that both orthogonal circular polarizations be received for the moon study program necessitated the use of some sort of fast-acting duplexing device in the high power transmission system. Because of the apparent impossibility of considering a scheme which would allow this duplexing device to be switched out during CW operation, it was necessary to design the system to handle the CW power as well as to perform the switching function in the short pulse lunar mode of operation. The successful use of a 100-kW circulator in the older R/C box lead to the development of a much smaller and improved ferrite circulator which could handle the 125-kW CW to be transmitted in each of the four legs of the high power transmission system. The circulator developed for the planetary radar installation is shown in Fig. 15 with its water cooled loads as it was initially installed in the system prior to the incorporation of the

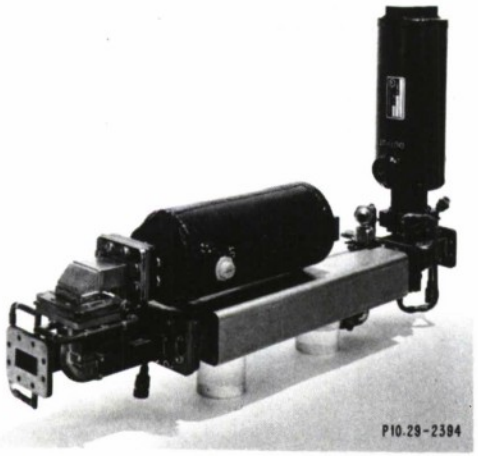

Fig. 15. Ferrite circulotor assembly with water cooled loads.

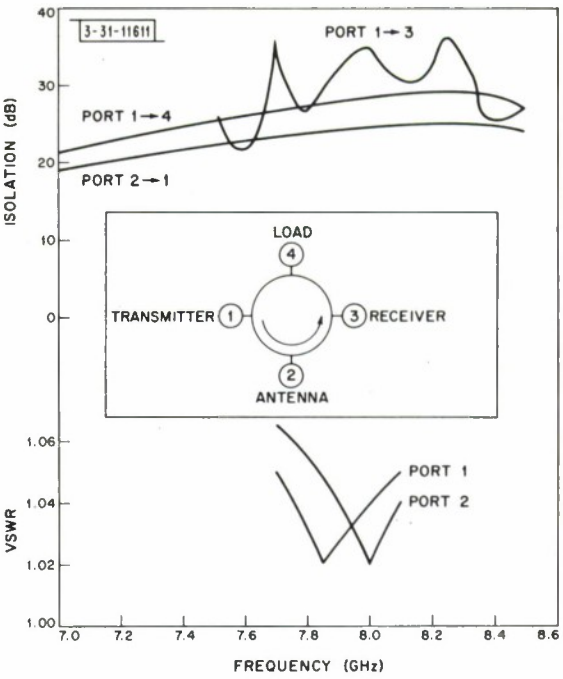

Fig. 16. Low level choracteristics of PXH-26 circulotor.

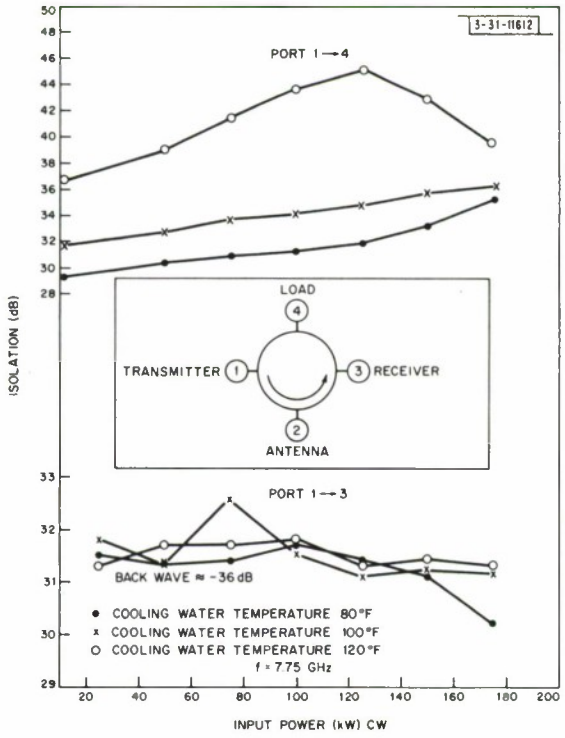

Fig. 17. High power charocteristics of PXH-26 circulotor.

orthogonal polarization reeeiving equipment. Upon installation of this equipment, the load lying parallel to the body of the eireulator was removed and eonneetion made to a hybrid summing network whieh eombined the outputs of the four eireulators. Figure 16 shows the low level isolation and VSWR eharaeteristies of the eirculator. The wide variations in isolation between ports 1 and 3 are due to the eombined effeets of the direetivity of the input hybrid and the mateh of the output hybrid. The isolation between ports 1 and 4 and between ports 2 and 1 are directly related to the differential phase shift variation with frequeney. Low level measurements show an insertion loss of 0.12 dB of whieh 0.03 dB is attributable to the hybrids. Calorimetrie measurements show a gradual inerease in loss with inereasing power level to a value of 0.16 dB at 175 kW CW. All units were tested up to this power level before installation.

The high power performanee of the eireulator is shown in Fig. 17. The important parameter here is the isolation between terminals 1 and 3 as this bears directly on the leakage expeeted at the reeeiver. It is seen that this isolation is for praetieal purposes independent of power level and temperature as would be expeeted because this parameter does not depend upon the differential phase shift properties. The baek wave in the resonant ring in which the rests were made was about 36 dB below the forward wave. This corresponds to a VSWR of about 1.03 which cheeks elosely with the low level measurements.

The measured isolation of 31 dB at 125 kW eould be as low as 27 dB, if the worst case combination of the eoupled field phase and the phase of the 1.03 mismateh were taken. With a termination VSWR of 1.2, the power eoupled to the receiver eould be, in the worst ease, only 17.4 dB below the transmitted power. At 500 kW CW this is 9 kW. The present system VSWR as seen by the eireulator is about 1.1; however, with a linear polarized feed this value would probably inerease to about 1.2 beeause the energy refleeted baek into the feed would now return through the high power lines. The RF system was designed with this eventuality in mind.

VI. RECEIVING SYSTEM

A. General Description

The reeeiving system is configured to perform both radar and radiometrie funetions. Provisions have been made for the reception of both right-hand and left-hand eircularly polarized signals using either masers or low noise parametric amplifiers as the prineipal aetive elements of the system. In the radar mode the system radiates right-hand eireularly polarized signals. The prineipal return, left-hand cireularly polarized, is reeeived direetly through the orthogonal summing network assoeiated with the feed system. The right-hand polarized return signals pass through the four eireulators and are summed in a hybrid network. During the initial phase of the planetary radar observations, only the prineipal return was reeeived, being amplified by a traveling-wave maser in a batch-filled helium dewar. For moon studies and Venus observations near inferior conjunction, it is desirable to simultaneously reeeive the two orthogonal eireularly polarized returns. Provisions have been made to aeeommodate two masers in a batch-filled dewar, but this eonfiguration will only be used if the operation of two masers in the Air Produets and Chemicals, Ine., elosed-eyele refrigerator proves to be impractical. For moon mapping purposes and for Venus observation at inferior eonjunetion, the return is strong enough to use low-noise parametric amplifiers.

The simplified block diagram of Fig. 18 shows how the system provides for three operating modes: (1) planetary radar, (2) moon observations, and (3) radiometry. In the planetary radar mode a very long high power pulse, 10 to 20 minutes in duration, is transmitted. The

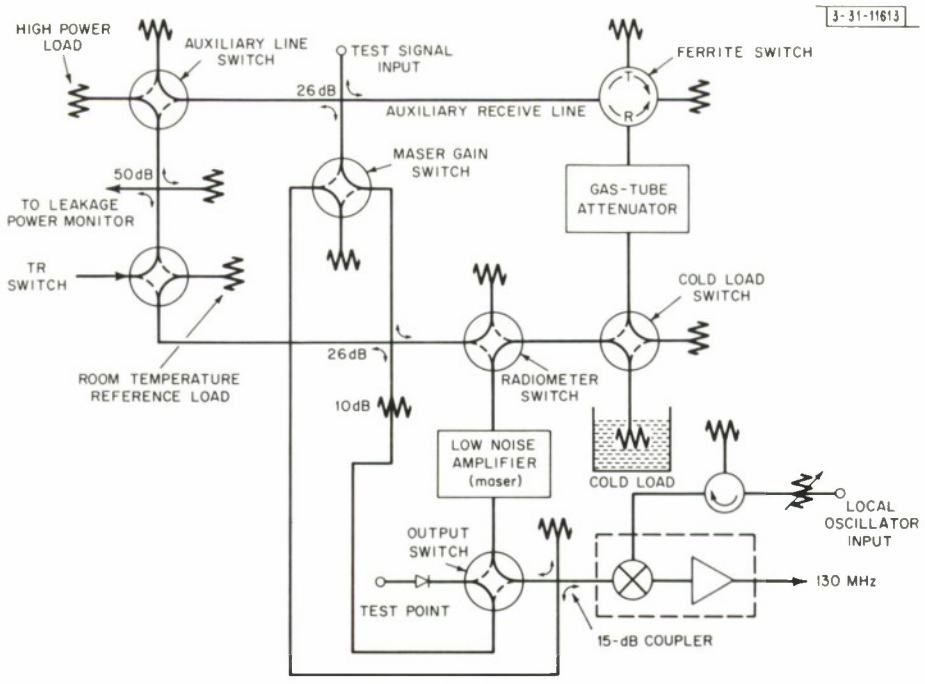

Fig. 18. Simplified diagram of principal polarization receiving channel.

auxiliary line mechanical switch is set to divert the leakage from the transmitter into the high power load. Both the TR switch (mechanical) and the radiometer switch (mechanical) are actuated in this mode, disconnecting the receiver when transmitting and providing isolation which reduces the average transmitter leakage into the receiver to −87 dBm. This is sufficient to prevent maser saturation which occurs at an average power of about −70 dBm. During planetary radar operation the cold load switch (mechanical) is positioned so as to reduce to a minimum the leakage to the receiver through the auxiliary receiver line. The transmission losses between the multimode horn and the maser input flange when receiving are shown in Table V.

For moon mapping, the transmitter operates at a high repetition rate, low duty cycle. Mechanical switching is far too slow for this mode of operation, so an auxiliary receive line has been incorporated which includes a ferrite switch and a pulsed gas-tube attenuator to protect the maser from transmitter leakage. The polarization decoupling in the feed network is 24 dB and the ferrite switch decoupling 22 dB. The isolation provided by the gas attenuator is a decreasing function of the incident peak power,* but is adequate in the power range used for lunar experiments to prevent maser saturation. The receive insertion loss for this operating mode is shown in Table V.

In the radiometer mode the TR switch is held in the receive position and the cold load switch is positioned to connect the cold load to the receiver. The radiometer switch is activated to alternately couple the antenna and the cold load to the maser receiver. The receiver losses for this mode are the same as for the planetary radar mode.

* Refer to Sec. VI-F which describes the pulsed gas attenuator.

TABLE V

PLANETARY RADAR RECEIVER LINE LOSSES

Campanent	Main Receiver Line Loss (dB)	Auxiliary Receiver Line Loss (dB)
Circular palarizer	0.012	0.012
OMT	0.02	0.02
3-inch waveguide	0.006	0.006
E-plane tee	0.008	0.008
20.7-inch waveguide	0.041	0.041
8-1/4-inch H bends	0.017	0.017
H-plane tee	0.010	0.010
TR switch	0.058	0.058
10-inch waveguide		0.02
Auxiliary line switch		0.08
3-1/2-inch waveguide		0.007
26-dB caupler		0.017
7-1/2-inch waveguide		0.015
Ferrite switch		0.11
8-1/2-inch waveguide		0.017
Pulsed attenuator		0.054
4-inch waveguide		0.008
Cold load switch		0.04
19-inch waveguide		0.038
17 flange jaints		0.012
Radiometer switch	0.058	0.058
10-1/4-inch twist	0.020	
26-dB directianal caupler	0.017	
7 flange joints	0.005	
Tatal Circuit Lass:	0.272	0.648
Naise Contributian (270°K enviranment)	17.2°K	40°K

The radiometer performs as calculated using the law of the radiometer[20,21]

$$T_{min} = \frac{K_1 T_s}{\sqrt{\tau B}}$$

where T_{min} is the minimum detectable temperature, $K_1 = 2$ is the receiver calibration constant for the Dicke radiometer, B is the predetection bandwidth, τ is the integration time, and T_s is the system temperature. This system, using the maser receiver, has proven to be an exceptionally good radiometer for observation of both the continuum and spectral lines.

B. Receiver Monitoring and Alignment

The receiving system has been provided with circuits which can be used to align the maser (or parametric amplifier) and to monitor and test the performance of the complete receiving system (see Figs. 18 and 19). To measure the gain of the low noise RF front end, signals from the swept RF generator are alternately fed into the maser input and the mixer preamplifier input by changing the setting of the maser gain switch. A precision RF attenuator in the sweeper is used to adjust the 130-MHz IF output to a constant value. For the nominal values of coupling shown in Fig. 18, the gain of the maser will be 11 dB plus the change in the precision attenuator setting required to maintain a constant IF level as the maser gain switch is actuated.

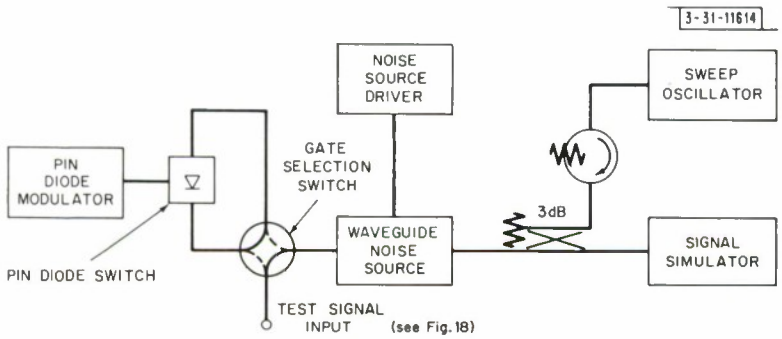

Fig. 19. Test circuit diagram.

A commercial waveguide noise source is provided for the measurement of receiver and system noise temperatures by the familiar Y-factor method. The noise level at the input to the low noise first stage may be accurately calibrated by comparison with the output of the liquid helium-cooled load.

A waveguide switch is interposed between the noise source and the couplers to the receiver lines. This waveguide switch permits a fast acting PIN diode switch to be inserted into or removed from the test line at will. The diode switch is employed for the injection of noise calibration pulses into the auxiliary receiver line during short-pulse operation of the radar.

The signal simulator provides a highly stabilized 7840-MHz signal for the purpose of calibrating the low noise stage. The output frequency is synthesized from stable signals at 100 and 30 MHz originating in equipment located at ground level and a 7710-MHz signal generated in equipment located in the PR box. The resultant 7840-MHz signal is fed through a precision attenuator into the receiver test line. Frequency and phase variation are accomplished at ground level by varying the frequency and phase of the 100-MHz signal. The 7840-MHz output level may be varied from the remote operating position over a 200-dB range. This is accomplished with a

0- to 99-dB programmable precision attenuator, variable in 1.0 dB steps, and two 40- and 60-dB attenuators which can be switched in or out by the operator. With this combination, any attenuation in steps of 1.0 dB can be obtained up to 200 dB. The simulator is more than capable of driving the first stage – from saturation to minimum discernible signal (–165 dBm in the case of the maser).

The simulator can also be used to generate RF pulses. This is accomplished by two solid-state switches in the 100- and 30-MHz lines, which are pulsed on and off simultaneously, thereby causing the 7840-MHz output signal to be pulsed.

To insure that no stray signals leak into the receiving system, all simulator components which may leak signals are packaged in a shielded enclosure.

The accuracy of the measurements made with a system using very low noise amplifiers depends upon an accurate knowledge of the effective noise temperature of the system and its components, particularly the low noise RF amplifier serving as the receiver front end. For the case of a maser front end, whose effective temperature can be as low as a few degrees Kelvin, it is desirable to be able to make noise measurements to an accuracy of ±1°K or better.

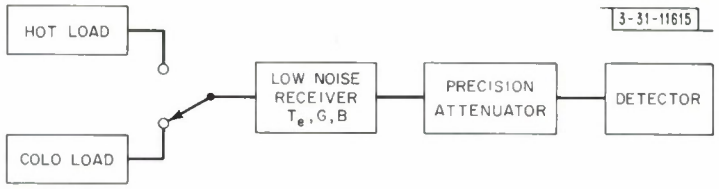

Fig. 20. Equipment configuration for determination of effective noise temperature T_e of a low noise receiver.

The noise temperature of an amplifier is determined by measuring the change of output power when two accurately known noise sources, T_H (hot source), and T_C (cold source), are alternately connected to the amplifier input as shown in Fig. 20. The ratio of the two output powers is known as the Y factor and is

$$\frac{(T_H + T_e)\,GBK}{(T_C + T_e)\,GBK} = Y = \frac{T_H + T_e}{T_C + T_e}$$

where B is bandwidth, G is the amplifier gain assumed here to be invariant during the time the measurement is being made, K is Boltzmann's constant equal to 1.38×10^{-23} watt-sec/°K, and T_e is the effective noise temperature of the amplifier. The Y factor is customarily read from a precision IF attenuator which is used to adjust the input to the detector to a constant value. The effective noise temperature of the low noise amplifier is then

$$T_e = \frac{T_H - YT_C}{Y - 1} \quad .$$

The absolute error introduced by the uncertainty in the actual temperature of the noise sources is found to be

$$(\Delta T_e)_H = \frac{T_H\,(T_C + T_e)}{T_H - T_C}\,\frac{\Delta T_H}{T_H}$$

$$(\Delta T_e)_C = \frac{T_C\,(T_H + T_e)}{T_H - T_C}\,\frac{\Delta T_C}{T_C} \quad .$$

The effect of inaccuracies in the knowledge of the temperatures of the hot and cold loads on the absolute error in the measurement of T_e is the same for both noise sources for the limiting case where $T_e \to 0$. However, for a finite receiver temperature, the contribution of error by the hot load increases more rapidly than that of the cold load as T_e grows larger. It seems prudent to be especially critical in choosing a hot load for precise measurements.

The precision of the measurement is affected by the accuracy with which Y can be determined as follows:

$$(\Delta T_e)_Y = \frac{(T_C + T_e)(T_H + T_c)}{T_H - T_C} \frac{\Delta Y}{Y} \quad .$$

Examination of this equation shows that if T_H is large compared to T_e, the change in the error ΔT_e is a slow function of T_H. The value of T_H should be chosen as high as possible consistent with maintaining a high degree of precision in the knowledge of its temperature. The error is an increasing function of T_C as T_C grows larger. The cold load temperature should, therefore, be kept small relative to the receiving noise temperature being measured.

Effects of change of gain are indistinguishable from errors due to the uncertainty with which the Y factor can be measured. This should be obvious from Fig. 20. Because the gain of an amplifier can be influenced by the impedance coupled to its input, care must be taken to ensure that the effects of mismatch variations between the two loads (both amplitude and phase) are negligible.

Once the low noise receiver has been calibrated and an accurate cold source incorporated in the microwave system, the effective system temperature can be measured in the same manner as the receiver calibration was made by measuring the Y factor when the receiver is switched between the antenna and the cold load.

For this case

$$Y = \frac{T_s}{T_C + T_r}$$

where T_s is the system temperature and T_C and T_r are the cold load and receiver temperatures, respectively.

The foregoing discussion of measurement errors has been restricted to factors important to the choice of hot and cold loads. More comprehensive discussions may be found in the literature.[22-24] Briefly stated, the hot load temperature should be much larger and the cold load temperature lower, if possible, than the temperature being measured. The accuracy with which these noise sources is known is of prime importance. In particular, the hot load choice should be based more on the accuracy with which its calibration is known than on obtaining a very high temperature.

For low noise receiver measurements, a hot load at room temperature and a cold load refrigerated at liquid helium temperature represent a good choice. There is little problem with a room temperature source which can be accurately known. However, a cold load which is accurately known is not a trivial device.

C. Maser

In order to achieve a system temperature of less than 75°K, it was necessary to select a preamplifier with a noise temperature of less than 25°K. At the time this choice was made, a maser was the only available amplifier that could meet this requirement in the frequency range

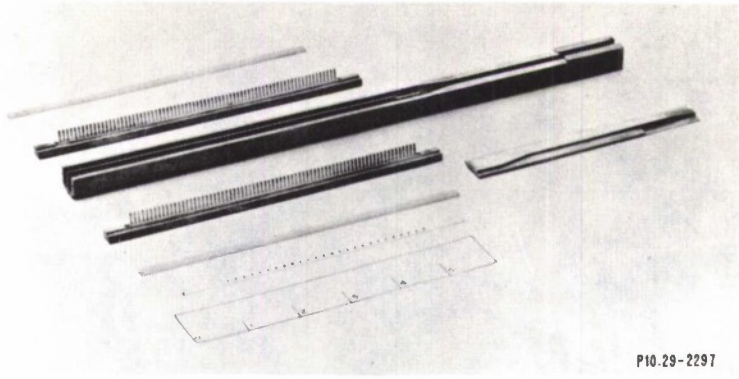

Fig. 21. Maser components.

7.500 to 8.000 GHz. As a result of competitive bidding, a contract was given to Microwave Electronics Corporation of Palo Alto, California, for a traveling wave maser amplifier. This work was subcontracted to Quantum Science Corporation, also of Palo Alto, which designed and constructed the maser.

The Haystack maser is of the traveling wave type,[25] employing a slow wave structure which couples the RF energy to the ruby material responsible for the maser action (see Fig. 21). Since there is no preferential direction in which amplification takes place in this type of maser, it is necessary to introduce nonreciprocal transmission elements in order to achieve a stable two-port amplifier. The nonreciprocal action is obtained through the unidirectional properties of a ferrite resonance isolator which is an integral part of the maser structure. The ferrite material, in the form of disks appropriately placed with respect to the comb structure (see Figs. 21 and 22) is chosen such that the field of the superconducting magnet associated with the maser is correct for gyromagnetic resonance in the ferrite material at the operating frequency. Reversal of the magnet field will, of course, reverse the directional in which amplification can take place.

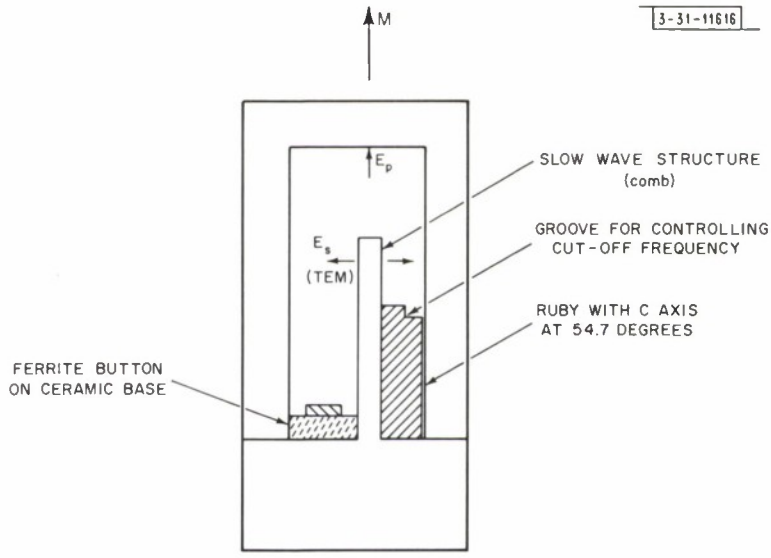

Fig. 22. Typical cross section of a traveling wave maser.

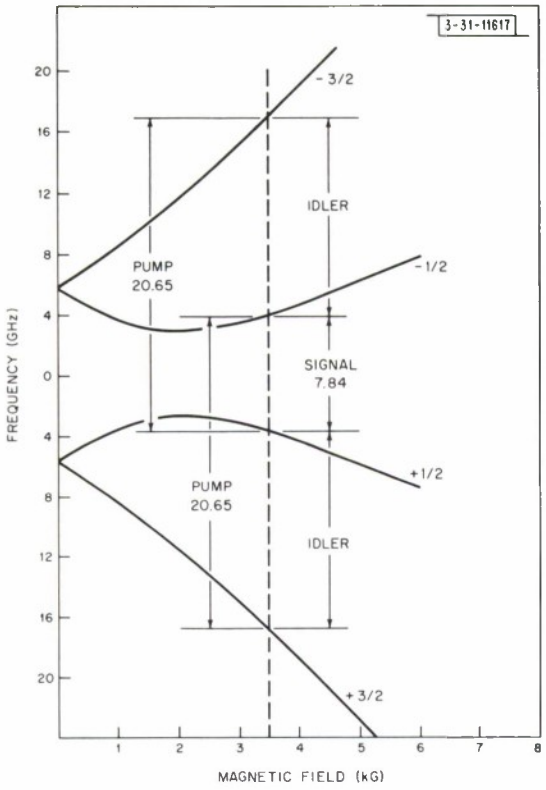

Fig. 23. Energy levels (frequency equivalent) for a ruby maser with the magnetic field at an angle of 54.7 degrees to the crystal C-axis.

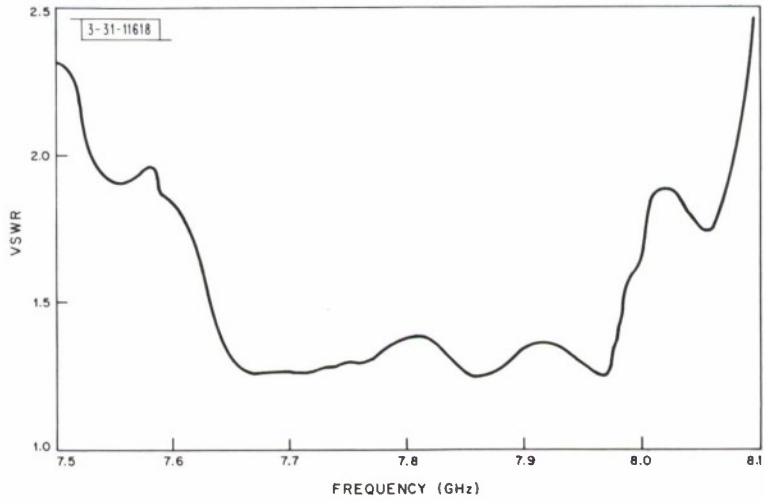

Fig. 24. Input VSWR of the maser amplifier at liquid helium temperature.

The active material employed in these amplifiers is Al_2O_3 with Cr^{+++} as the paramagnetic impurity ion. The ruby material is ground so that the principal optical axis (C-axis) is at 54.7 degrees (thc "double pump" angle) with respect to the applied magnetic field. The four paramagnetic energy levels for ruby at this orientation are shown in Fig. 23, where the energy level is given in terms of its frequency equivalent.

Two important parameters determine the magnitude and uniformity of the gain throughout the relatively long 6-ineh active region in the maser structure: (1) the variation in chromium concentration throughout the ruby material, and (2) the crystal orientation quality. The ruby employed in these amplifiers was grown by the Czochralski method which is capable of produeing large size erystals of excellent structural eharacteristics. The uniformity of the C-axis orientation in this material was measured to be fractions of a tenth of a degree rather than the 1/4- to 1-degree misorientation typical of materials grown by the flame fusion method. At the 54.7-degree orientation, misalignment of the crystal axis by 0.1 degree causes a shift in the center frequency of the ruby line of more than 10 megaeyeles. The gain over a 6-ineh ruby seetion is three to four times higher with the Czoehralski grown material than with good quality flame-fusion grown ruby.

The eomb structure in the Haystack maser has a passband of 2 GHz. Operation is limited to less than half of this range by the input mateh shown in Fig. 24. Because of the symmetry of the dcvice, the output VSWR is essentially the same as the VSWR at thc input. A transition from waveguide to the maser input having a VSWR of less than 1.2 over the 2-GHz band has been designed for future use.

The instantaneous bandwidth is determined by the ruby line width. This can be varied a certain amount at the expense of gain by varying the magnetic field along the length of the ruby. The superconducting magnet contains trim coils which ean be energized to produee magnetic field variations for the purposc of bandwidth adjustment. For radar operations the narrow band configuration is adequate, typically a 13-MHz bandwidth with a gain of 37 dB. For radiometer applications, the maser is frequently tuned for a wider bandwidth. Table VI shows the parameters measured during the acceptance tests.

TABLE VI
OPERATING CHARACTERISTICS OF THE HAYSTACK MASER

Signol frequency	7840 MHz
Pump frequency	20,640 MHz
DC mognetic field	3460 Gauss
Gain	30 dB
Bondwidth (3 dB)	22 MHz
Input saturotion power (for 0.5-dB goin compression	−68 dBm
Gain instability — short term, 5 min	0.05 dB
Gain instobility — long term, 8 hr	0.15 dB
Gain instobility during motion (± 45° from the verticol)	< 0.20 dB
Noise temperoture	8.0 ± 2.0°K

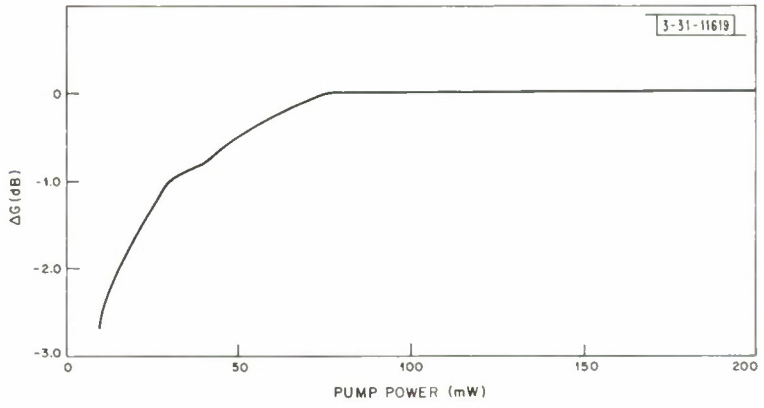

Fig. 25. Gain change versus pump power at 7.840 GHz.

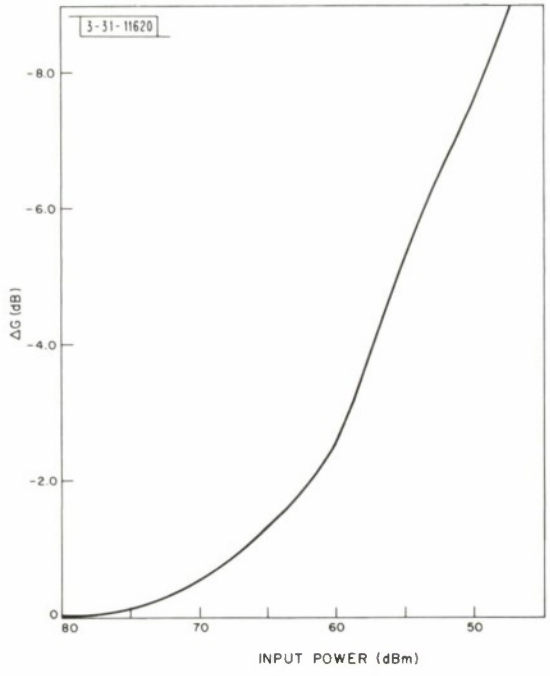

Fig. 26. Gain compressian versus input pawer at 7.840 GHz far an amplifier gain of 30 dB.

Gain changes are very important in both radiometer and radar use of the receiving system. Unlike the parametric amplifier, maser gain is virtually independent of pump power if this power is greater than a critical value, as shown in Fig. 25. The maser is, however, easily saturated and has a very long time constant. This saturation is due to the depletion of the higher energy state by a large signal. Figure 26 shows the gain compression for a strong signal at the operating frequency. Figure 27 shows the effects of strong out-of-band signals on maser gain.

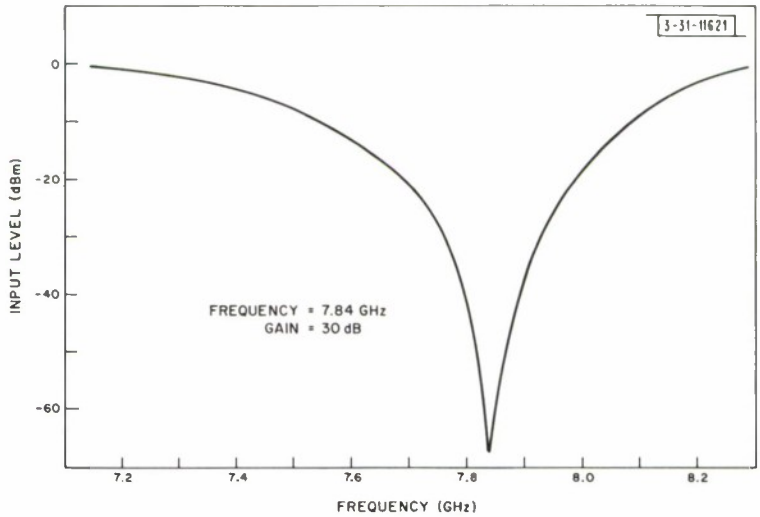

Fig. 27. Out-of-band power level that compresses gain of the maser 0.5 dB (freq = 7.840 GHz, gain = 30 dB).

The first maser, which is mounted in the helium dewar (see Fig. 28), and whose performance is shown in Table VI, contains two 6-inch ruby sections and provides considerably more gain than required. This excess gain is due to the exceptionally high quality ruby material which became available after the maser design had been committed. A single six-inch ruby will provide adequate gain to satisfy the Haystack radar requirements if the bandwidth of the structure is reduced to about 500 MHz. Two additional maser units, each containing a single 6-inch ruby, with their superconducting magnets, have been procured and are being installed in the Air Products and Chemical, Inc., closed-cycle refrigerator shown in Figs. 29 and 30. This assembly will replace the batch-cooled dewar now in use in the PR box and provide two receiving channels for those experiments requiring the reception of the two orthogonal polarizations. The dewar mounted maser will be used for radiometry experiments, a purpose for which it is better suited than the refrigerator mounted maser because of its wide tuning range and greater instantaneous bandwidth capability.

One problem of refrigerator operation of masers is the requirement to maintain the maser temperature constant to about 0.01°K. This stringent requirement arises because a temperature change of 0.1°K will result in a maser gain change of 1.0 dB. The Air Products refrigerator has been provided with a temperature controller which will meet this requirement.

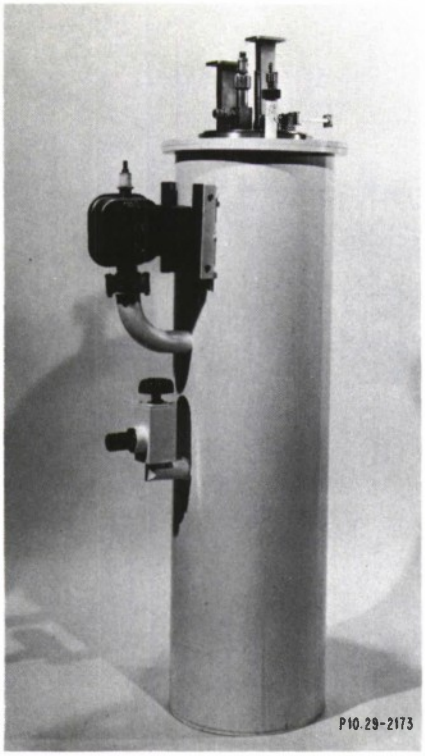

Fig. 28. Helium dewor with moser instolled.

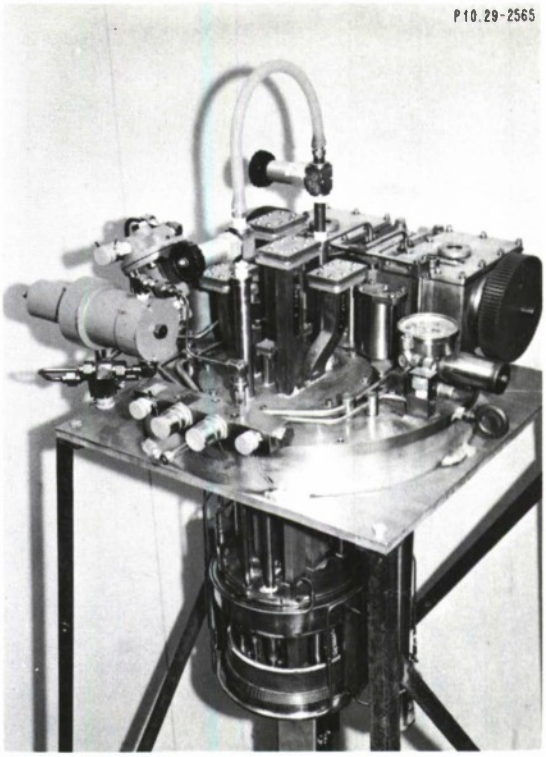

Fig. 29. Air Products refrigerator (top view with vocuum jacket removed) showing woveguide correction for two mosers.

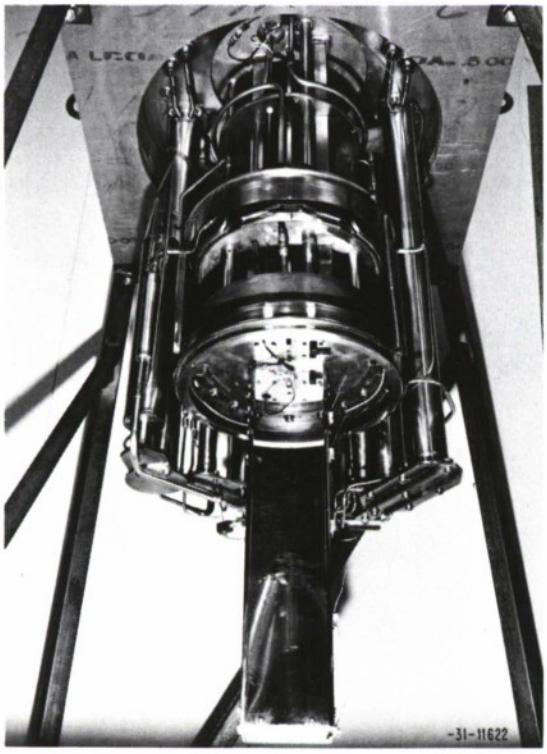

Fig. 30. Photogroph of Air Products refrigerotor (bottom view with vocuum jocket removed) showing one moser in ploce.

D. Cold Load

The requirement for calibration of the Haystack system noise level with an accuracy of a few degrees Kelvin, and for furnishing a stable reference load for the radiometer, dictated the choice of a liquid helium cooled load rather than a commercially available load cooled by liquid nitrogen. Several workers[22,26,27] have reported on successful helium cooled load designs which were employed either for system calibration purposes or for the evaluation of maser amplifiers. The Haystack liquid helium cooled load design was based on the experience of these workers, and follows for the most part, the designs of Eisle[22] and Penzios.[27]

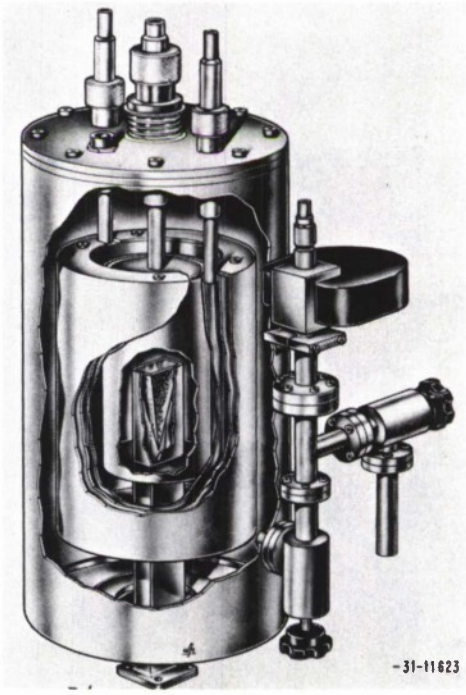

Fig. 31. Cut-away view of Haystack cold load.

Figure 31 shows a cut-away of the cold load. The load itself is a spear of lossy material contained in an evacuated waveguide which is in contact with the liquid helium. The helium container is surrounded by a vacuum jacket, a nitrogen container, a radiation shield and another vacuum space. The waveguide connecting the load to the room temperature environment is of thin walled stainless steel for thermal isolation. The inner walls of the waveguide are electroplated with a thin layer of copper to reduce the RF losses. The waveguide vacuum window consists of a thin mylar sheet which is clamped at the bottom of the liquid helium container.

The effective load temperature at the input flange was determined both by calculation and by comparison with a known standard. In order to determine the thermal parameters neeessary for the temperature calculations, a prototype load was built in which a number of thermocouples were attached to the waveguide and buried in the load material itself. The cold load temperature has been determined to be 33°K when cooled with helium and 88°K when cooled with nitrogen. The hold time with helium cooling is approximately 4 hours with the limitation of the 1-liter capacity of the helium dewar. The hold time with nitrogen cooling is over 8 hours.

TABLE VII

INSERTION LOSS OF CHOKELESS SWITCHES AT 7.84 GHz

Switch	Loss at 7.84 GHz (dB)	Approximate Frequency at Peak Loss (GHz)	Notes
Chokeless			
Model WSO 2H11			
Serial No. 502	0.013	8.9	
Serial No. 503	0.015	8.9	~0.012 dB at 7.5 GHz
Model WSO 2H13	0.018	9.0	~0.02 dB at 7.5 GHz
	0.023	9.0	
	0.026	9.0	~0.035 dB at 7.5 GHz
	0.027	9.1	

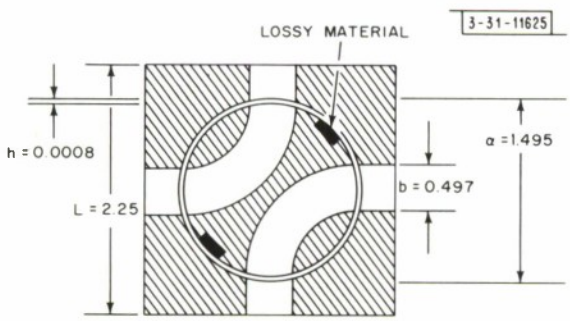

Fig. 32. Chokeless switch configuration.

The temperature achievable in a cold load is strongly dependent on the load material. The Haystack load uses a composition material which is inexpensive, is relatively easy to fabricate into a well matched load, and is well behaved at low temperatures. Its principal disadvantage lies in the fact that it is a poor thermal conductor and consequently cannot be cooled to the 4.2°K of the helium bath. Experience has shown that the actual temperature of this type of load is about 10°K above the temperature of the liquid helium. A load which efficiently conducts heat to the helium bath can be constructed, but with a great deal more difficulty and expense. Eisle used ruby which had been coated with nichrome, having a film resistivity of 500 ohms/square. Ruby is a good thermal conductor at liquid helium temperatures. There are other possible choices of material for constructing cold loads such as synthetic sapphire, beryllium oxide, and perhaps polycrystalline aluminum oxide.

The Haystack cold load is suitable for the purposes for which it was intended, but its effective temperature is somewhat higher than desired for an accurate determination of the effective noise temperature of a maser amplifier.

E. Mechanical Switches

The RF switching requirements for both the planetary radar mode of operation and the radiometer observation allow the use of mechanical switches. The familiar four-port transfer switch is best suited for these applications which require that a waveguide port be alternately connected to one of two other waveguide ports.

The performance of the switch during the short switching interval is unimportant, but the circuit must be well-matched and have a low insertion loss at all other times. For planetary radar use the switch must also be capable of handling the transmitter leakage which is less than 5 kW CW for full power operation.

A number of different commerically available switches have been evaluated for use in the Haystack system. Attention was focused on the insertion loss which varied widely among the various switch types tested. Typical data are shown in Table VII for chokeless switches which gave the best low loss performance in the 7.5 to 8.0 GHz frequency range. This type switch design relies on a very close spacing between the rotor and stator to minimize the coupling out of the main waveguide channel and on lossy material placed in the rotor to achieve high values of circuit isolation. Figure 32 shows the basic design configuration, and Fig. 33 the equivalent microwave circuit for this type switch.

A characteristic observed in both choked and unchoked switches is that there is a fairly broad low loss region followed by a rather sharp high loss peak. In some switch designs this peak occurred near the Haystack operating frequency. For the chokeless switch design used, the loss peaked at about 9 GHz as shown in Fig. 34. Calculations of switch loss based upon the equivalent circuit of Fig. 35 agreed quite well with measured results, as shown in Fig. 36, when the proper values of loss and electrical path length were assigned to the transmission path formed by the gap between the switch rotor and stator. This path is not a simple waveguide because there is coupling around the top and bottom of the rotor through the mechanical clearance. One switch rotor was lathe turned to successively smaller diameters in order to measure the effect of varying the clearance gap dimension.

Experiments were also conducted in an attempt to improve the performance of switches employing chokes in the stator, but in no case did the insertion loss reduce to as low a value as

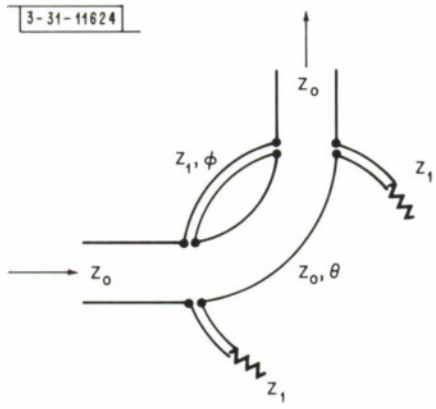

Fig. 33. Equivalent circuit of switch.

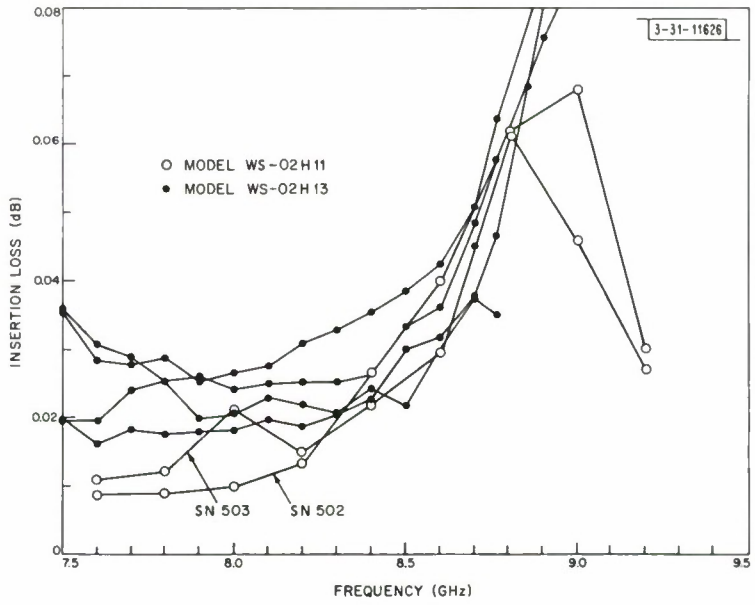

Fig. 34. Insertion loss for several chokeless switches.

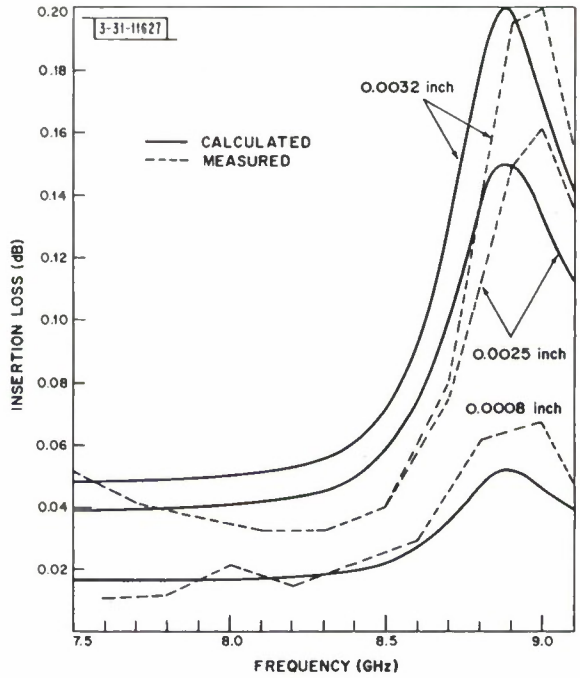

Fig. 35. Comparison of calculated and measured results for several ratar gap spacings.

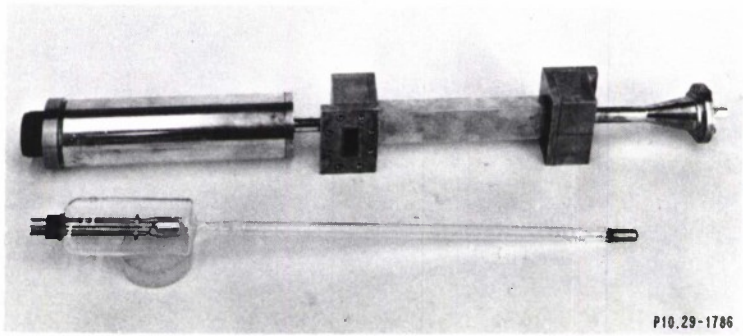

Fig. 36. Pulsed gas attenuatar as originally designed for the Haystack radar.

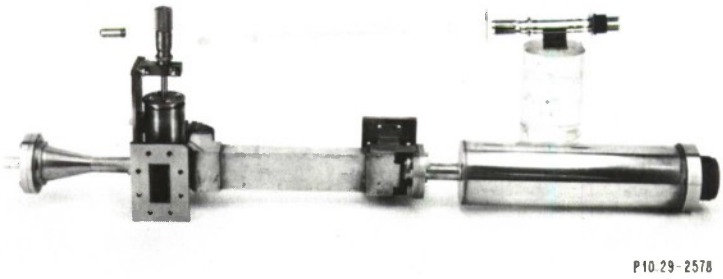

Fig. 37. Improved pulsed gas attenuator.

obtained for the chokeless switches. Problems of higher order mode resonances were encountered in the chokes and difficulty was experienced in obtaining a good broadband match in some cases.

High power tests of the chokeless switches were conducted up to the 5 kW, CW level without encountering either electrical or mechanical problems. It was observed that the switch rotor became too hot to touch at the highest power levels, indicating that some form of cooling should be incorporated for any application requiring the transmission of still higher power.

F. Receiver Protection – Gas Attenuator

The block diagram of Fig. 19 shows how the receiving system has been configured to allow rapid changeover from the long pulse planetary mode of operation to the short pulse lunar mapping mode. For this short pulse mode, with its relatively high pulse repetition frequency, a fast acting transmit-receive switch is required to isolate the receiver from the transmitter during the interval when high power RF is being radiated. The mechanically operated switch used for planetary radar purposes is much too slow to be useful. The scheme shown in Fig. 19 employs a Ferrotec Model R-521-LS ferrite switch in WR-112 waveguide connected in tandem with a gas tube attenuator[28] designed at Lincoln Laboratory (see Fig. 36). A more recent pulsed attenuator development (see Fig. 37) makes it possible to provide adequate receiver protection without the use of the ferrite switch. This device will be incorporated in the system during a future modification. The switching time for the ferrite switch is 150 μsec to the 90 percent recovery point and is determined by the time constant of the magnetizing solenoid. The gas attenuator requires about 100 μsec to stabilize when the plasma discharge is turned on. When the discharge is turned off, the recovery time to 3-dB insertion loss is about 250 μsec. Full recovery takes place within 375 μsec. Some of the characteristics of the ferrite switch and of the pulsed attenuators are shown in Tables VIII and IX.

In the lunar mapping program, the pulse length used may vary from 5 to 20 μsec depending upon the area of the moon being mapped. The repetition frequency is determined by limitations imposed by the computer and does not exceed 100 pps at the present time. The highest possible duty factor that can be encountered is therefore 2×10^{-3}.

The average power at which the maser gain is compressed by 0.5 dB is −70 dBm. The maximum peak transmitter leakage at the worst obtainable duty factor could therefore be as high as −43 dBm without seriously affecting maser performance.

TABLE VIII FERRITE SWITCH CHARACTERISTICS*	
Isolation	> 25 dB from 7.7 to 8.1 GHz 30 dB at 7.84 GHz
Insertion loss	< 0.25 dB from 7.7 to 8.1 GHz < 0.15 dB at 7.84 GHz
VSWR	< 1.2 from 7.7 to 8.1 GHz
Recovery time	150 μsec to 90 percent
* Coil current = 350 mA (manufacturer's data)	

TABLE IX PULSED ATTENUATOR CHARACTERISTICS	
Isolation	Varies with incident power (see text)
Insertion loss	0.04 dB (old model) 0.07 dB (high power model)
VSWR (receiving)	< 1.15 from 7.7 to 8.0 GHz (old model) < 1.15 tunable (high power model)
Recovery time	< 250 μsec (3 dB) < 375 μsec (full recovery)

The leakage from the high power transmission system into the receiving system is less than 5 kW peak when the transmitter is operating at full power (500 kW peak). In the case of the principal polarization receiving circuits this leakage has been measured to be less than 2 kW peak and is reduced to less than 2 watts peak at the input of the pulsed attenuator by virtue of the isolation afforded by the ferrite switch. The pulsed gas attenuator is a very nonlinear device as is evident from its leakage characteristics shown in Figs. 38 and 39. Because of this extreme nonlinearity it is unwise to extrapolate performance much beyond the known performance region.

In order to understand the principal of operation of the pulsed gas attenuator, it is instructive to consider a simple model consisting of an elementary transmission line composed of series inductance and shunt capacitance in which a portion of the capacitive element will consist of a plasma.

The propagation constant for such a line is written as

$$\gamma = \sqrt{ZY} = j\omega\sqrt{LC} \quad .$$

The plasma may be considered as an admittance A_p loading the line

$$A_p = \frac{KIe}{v_d m(\nu_c + j\omega)}$$

where e and m are, respectively, the charge and mass of the electron, ν_c is the collision frequency, I is the total current, v_d is the electron drift velocity, and K is a factor which takes into account the fact that the plasma does not fill the whole volume of the transmission line.

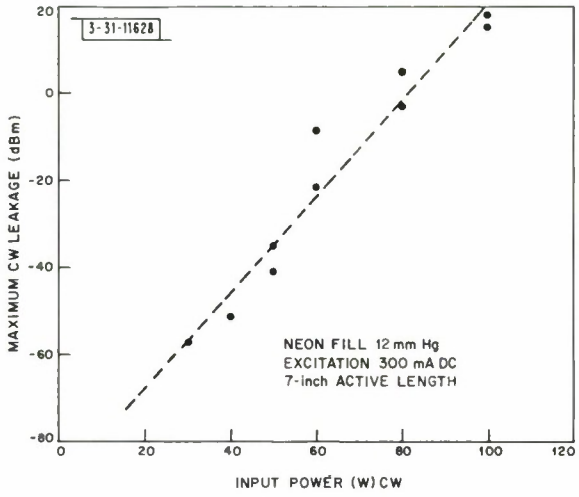

Fig. 38. Pulsed attenuatar CW leakage characteristic.

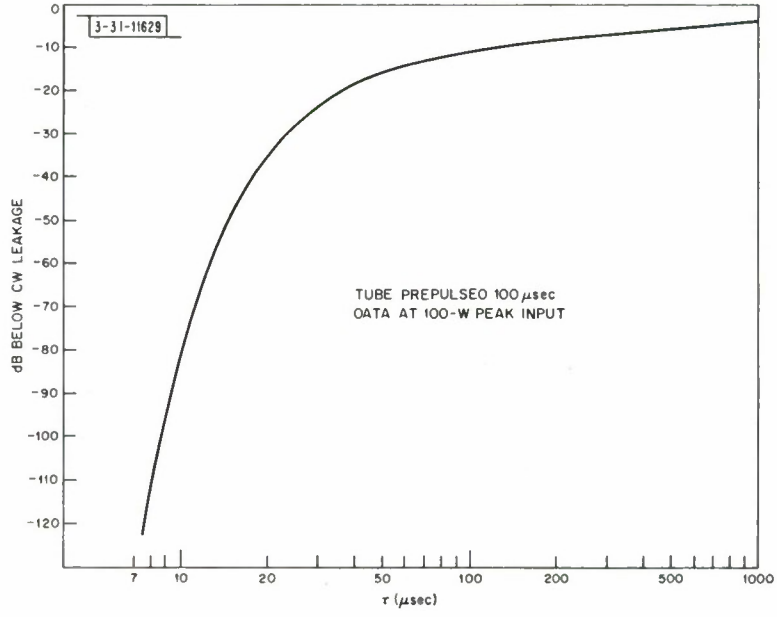

Fig. 39. Pulsed attenuatar leakage characteristic.

The propagation constant may be written

$$\gamma = [j\omega L(j\omega C + A_p)]^{1/2}$$

and becomes

$$\gamma = \omega\sqrt{L}\left[\left(\frac{KIe}{v_d m(\nu_c^2 + \omega^2)} - C\right)^2 + \left(\frac{\nu_c/\omega KIe}{v_d m(\nu_c^2 + \omega^2)}\right)^2\right]^{1/4} (\cos\Phi + j\sin\Phi)$$

where

$$\Phi = \frac{1}{2}\tan^{-1}\left(\frac{\nu_c/\omega KIe}{KIe - Cv_d m(\nu_c^2 + \omega^2)}\right) .$$

This equation is valid for generalized TEM transmission line when the plasma density is not high enough to perturb the electric field. Actually, the pulsed attenuator plasma does greatly perturb the ficlds, which, coupled with the fact that waveguide modes are involved, makes the problem a great deal more complex. However, the relationship given here does, in a simple way, describe the phenomena responsible for the behavior of the device.

If the collision frequency ν_c is allowed to go to zero, which would correspond to an electron gas, the transmission line becomes cut off when $KIe/v_d m\omega^2 = C$ and will not propagate in the usual sense for values of current larger than the critical current. This is the basic phenomenon responsible for the behavior of the pulsed attenuator. The presence of gas in the tube provides a neutral plasma and an easily attainable high electron density. It also provides a loss mechanism which modifies the behavior of the attenuator in much the same way as a resistor damps, or lowers the Q of a tuned circuit. As the current increases and the plasma resistance becomes lower, the waveguide with the plasma-filled tube along its center line begins to appear as a coaxial line with the plasma being a lossy center conductor whose loss is decreasing as the current increases. The waveguide partially filled with plasma is actually a very complex transmission system. The very nature of the device as it is realized in practice provides strong coupling to the TEM mode at the transition between the normal waveguide and the waveguide which is partially filled with plasma. A cross section view of the pulsed attenuator is shown in Fig. 40. The series impedance represented by the plasma is

$$Z = \frac{v_d m(\nu_c + j\omega)}{Ie} \text{ ohms/unit length} .$$

The shunt susceptance due to the capacitance per unit length of the plasma center conductor to

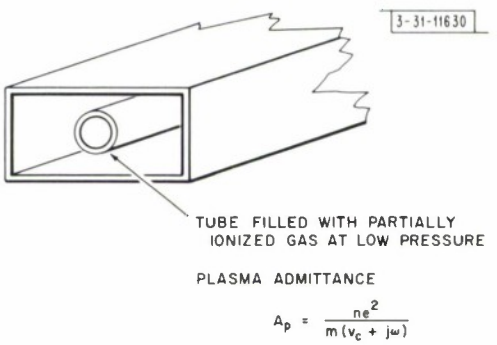

Fig. 40. Cross section of a pulsed ottenuotor.

the waveguide walls is $\gamma = j\omega C$. The propagation constant for the coaxial TEM mode becomes

$$\gamma = \sqrt{\frac{\omega C v_d m}{le}} \left(\nu_c + \omega^2\right)^{1/4} (\cos \Phi + j \sin \Phi)$$

$$\Phi = \frac{1}{2} \tan^{-1} \left(- \frac{\nu_c}{\omega}\right) \quad .$$

The attenuation in the TEM mode is represented by the real part of the above expression. At high currents, where propagation in the TEM mode is expected, the attenuation should go inversely as the square root of the current. The attenuation characteristic of the neon-filled tubes used at Haystack is shown in Fig. 41. The attenuation falls off at high currents as expected.

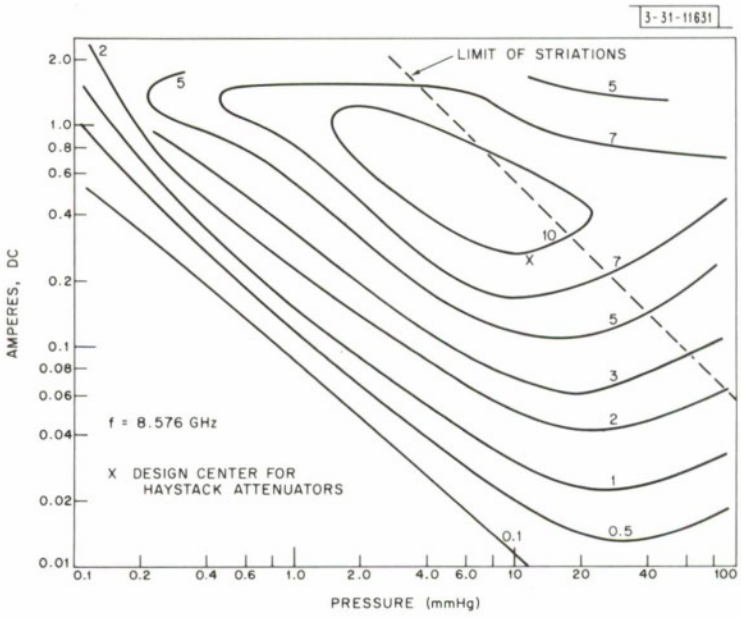

Fig. 41. Contours of constant attenuation (dB/cm) for neon-filled attenuator.

The attenuation data shown in Fig. 41 is for the small signal case where the RF leakage energy is not sufficient to contribute noticeably to the plasma density. For the practical case, the leakage heats the plasma and increases the electron density. This has the same effect as locally increasing the DC current I by a considerable amount, thus reducing the attenuation by making the plasma tube a better conductor to the TEM mode. The time constant for this reduction of attenuation by RF heating is quite long and is related to the propagation velocity of the warm plasma along the tube. The effect can be seen in Fig. 39 where attenuation is plotted as a function of pulse length.

In the steady state the plasma density will be highest at the input to the attenuator and will decrease along the tube as the RF amplitude is attenuated to the value where the small signal characteristics are reached, from which point the maximum attenuation is again realized. As the RF power is increased this point is arrived at farther along the tube. For the Haystack attenuator, the warm plasma region seems to lengthen by about 2 cm for each 1-dB increase in power. This occurs for an input power of 10 to 20 watts.

A second limitation on pulsed attenuation operation is due to the heating of the tube by both the DC current which sustains the plasma and the RF leakage from the transmitter. A maximum tube temperature of 300° C should not be exceeded. Figure 42 is a graph of temperature measured at the RF input end of the quartz tube by thermocouples placed on the bulb.

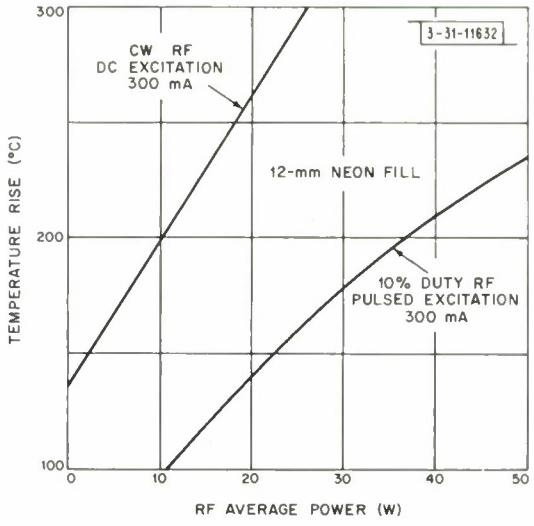

Fig. 42. Temperoture of quortz tube.

For pulse lengths longer than about 20 μsec at the 0.002 duty factor, or with longer pulse lengths at higher duty factors which may be encountered in future experiments, it is necessary to provide some kind of high power limiter in front of the pulsed attenuator. The Ferrotec switch is currently used, but a scheme has been devised and will be employed in the future in which the pulsed attenuator gas tube is used both as an attenuator and a power sensitive reflecting element. The configuration of this circuit is shown in Fig. 43. The quartz plasma tube passes through a low Q cavity formed from a section of normally cut-off waveguide which is resonated by the presence of the quartz. With a loaded Q of 15, and an active attenuator length of 6 inches, the overall cold insertion loss of the gas protector is about 0.07 dB. The leakage power as a function of peak input is shown in Fig. 44 and the heating as a function of average input is shown in Fig. 45. The leakage is a little higher than anticipated from a knowledge of the performance of the protector cavity and attenuator taken separately. It is believed that there is significant coupling between the two elements via the plasma tube, which would act as a lossy coaxial line. The proper placement of chokes would probably reduce this coupling. This will be tried, but the present design is adequate for foreseeable experiments and will eliminate the more lossy ferrite switch.

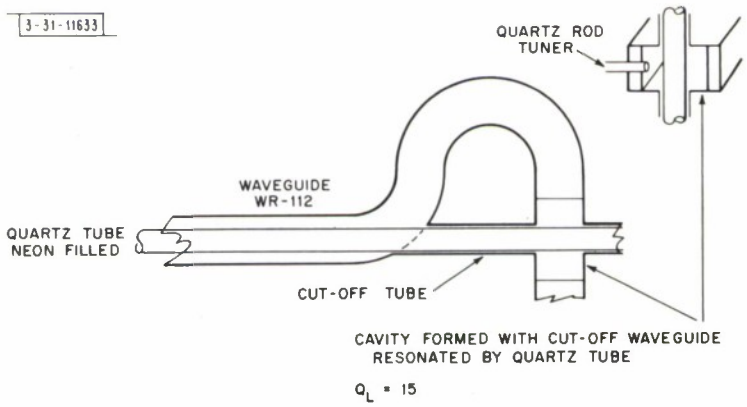

Fig. 43. Cross section of high power gos attenuotor.

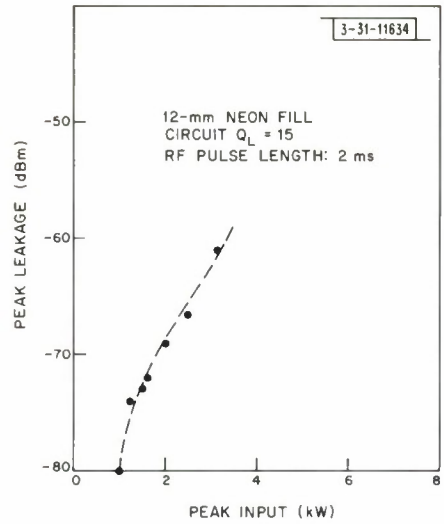

Fig. 44. Measured leakage characteristic of high power gas attenuator.

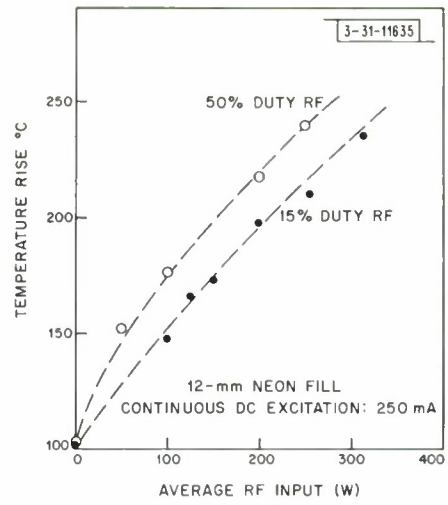

Fig. 45. Measured temperature rise of high power gas attenuator.

G. Feed System

1. Requirements

In its original concept the Haystack system was to provide facilities for both radar and communications experiments. The proposed communications experiments, which were later dropped from the program, required an autotrack mode in which the antenna would follow the apparent source of incoming radiation. The original design of the Haystack feed incorporated a tracking capability, but the achievement of this capability was subordinated to the requirement to achieve near optimum performance in the signal channel. The same basic feed design was ideally suited to the planetary radar program because of the excellent main beam characteristics achieved, i. e., high gain, low sidelobe level and high efficiency. Furthermore, the four-pipe excitation which had originally provided the tracking capability allowed division of the 500-kW transmitter power into four separate waveguides, thus alleviating a potential transmission line problem that might have otherwise existed.

It is well known that for monopulse tracking antennas the requirements for optimizing the sum channel and tracking channel performances are in conflict with one another. The four-horn feed, for example (which, incidentally, because of its well known characteristics, will be mentioned frequently as a standard of comparison), suffers rather seriously in two distinct areas: (1) the maximum efficiency in the sum mode is reduced because of the presence of the dividing septa which lie in the E-plane, and (2) the horn aperture size for optimum tracking performance is about double the size required for optimum sum efficiency. The familiar twelve-horn[29] and five-horn designs can offer some improvement or at least different trade-offs but it is clear that what is desired is some method which permits independent control of sum and difference radiation patterns. The approach taken in the design of the Haystack feed is to use a single horn in which the sum and difference patterns are generated with higher order modes which are excited at the horn throat. This multimode horn does not solve all the problems involved in the design of the ideal tracking feed, but it does offer the best trade-offs for fulfilling the Haystack Planetary Radar requirements in that its sum beam efficiency and the antenna temperature are both improvements over what is achievable with the above mentioned multihorn feeds.[30]

The Haystack feed system behaves much like a four-horn monopulse system up to the point where the higher order modes are generated, the two being identical in their microwave sum and difference networks. The orthogonal mode transducers and the circular polarizers are conventional. A cluster of four of these circuits excites the four square apertures of the horn throat, thus generating the circular polarization excitation for the multimode feed. This is shown schematically in Fig. 46.

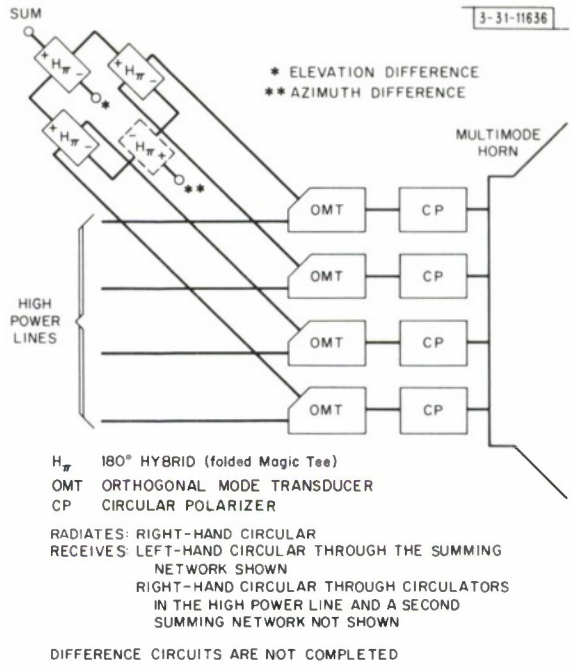

Fig. 46. Haystock feed system.

2. Multimode Horn

A feed aperture distribution consisting of a superposition of waveguide modes makes it possible to exercise a certain amount of independent control of the sum and difference radiation patterns if the amplitudes and phases of the required modes can be controlled. The number of modes which can be generated and controlled in any practical design is quite limited, but even with only a few modes, substantial improvements can be obtained in feed performance over conventional feeds.[31-37]

The multimode feed, Fig. 47, is basically a square pyramidal horn fed by a cluster of four waveguides. Quadrature symmetry is preserved throughout to permit either dual or circular polarization operation. The design objective is to use only the following waveguide modes: the TE_{10}, TE_{12} and TM_{12} modes in the sum channel, the TE_{11} and TM_{11} modes for E-plane tracking, and the TE_{20} mode for H-plane tracking.

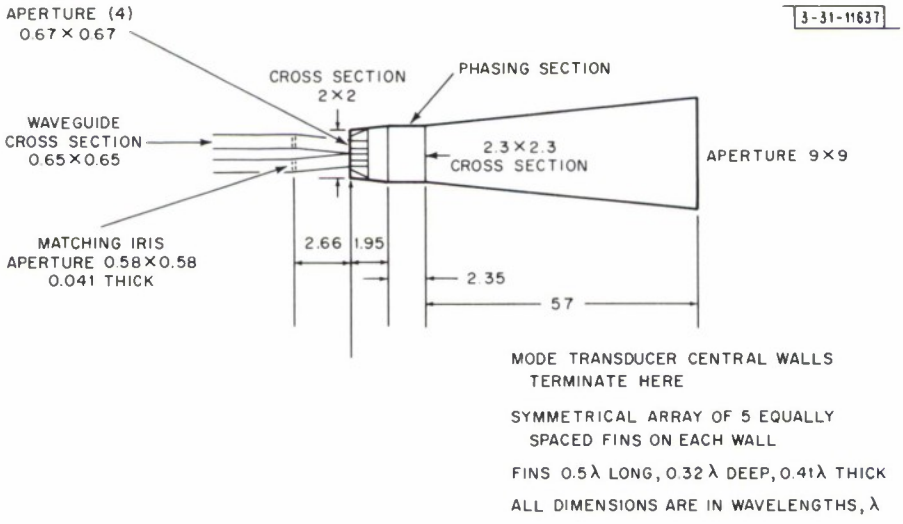

Fig. 47. Longitudinal section of high power duol-polarized multimode feed horn.

Figures 48(a) and (b) show the resultant E-field configurations for these mode combinations when the component modes are combined in the most favorable phase. From these it is easy to visualize the principle which permits the observed performance of the multimode feed. The most important feature of the horn design is the achievement of taper in the E-plane by introduction of the TE_{12}, TM_{12} pair which results in low sidelobes and increased sum beam efficiency. The degree of taper is adjusted to equalize the E- and H-plane pattern beamwidths. Theoretically, the percentage of power contained within the main beam of this feed is 97 to 98 percent. By way of comparison, the four-horn feed has only 69 percent of the power in the main beam.

Higher order modes are generated in a waveguide transmission system at points of either abrupt or progressive change in geometry. Even the simplest geometrical configurations are difficult to handle analytically. The tracking multimode horn in its final form is so complex as to discourage analysis, but it is possible to break down the problem so that a considerable amount of design analysis can be performed and the overall performance understood in a qualitative way.

The sum beam is generated by exciting the four waveguides entering the horn throats with waves of equal phase and amplitude. This produces a distribution at the horn throat discontinuity which is double-cosine in the H-plane and uniform in the E-plane. The boundary conditions require that in the plane of the throat discontinuity the E-field be zero at the septum formed by

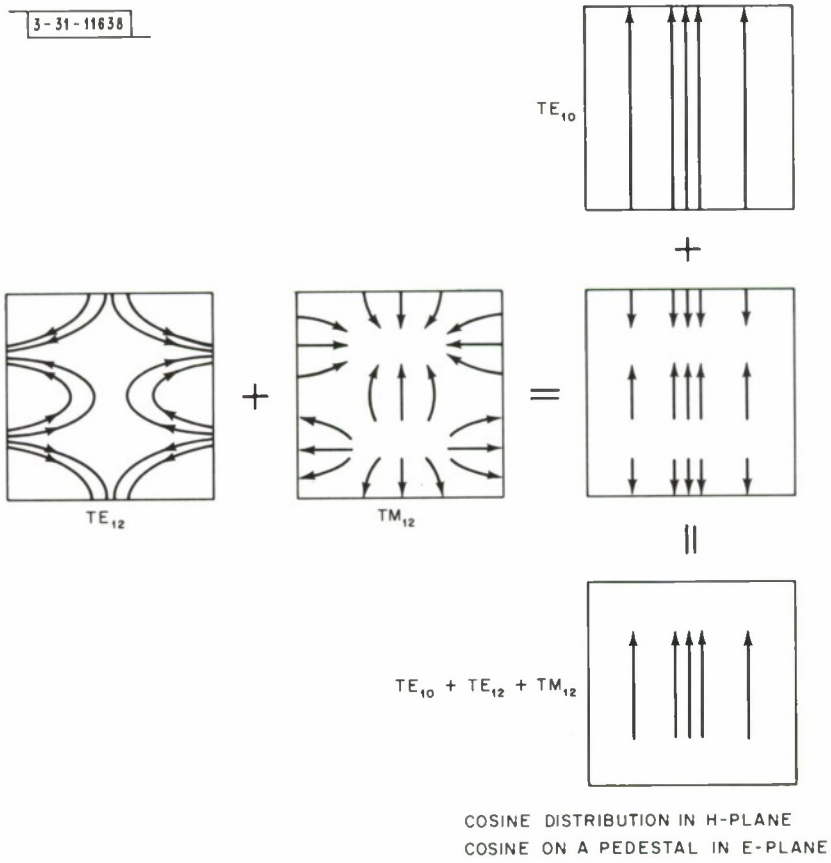

Fig. 48(a). Modes responsible for forward, or sum, beam.

the eommon waveguide walls whieh lie parallel to the E-field, Fig. 49. This tends to strongly excite the TE_{30} mode. The step at the outer walls generates the TE_{30} at about the same intensity as the septum, but in anti-phase.[38] The two contributions of TE_{30} which are generated in the same transverse plane, almost eompletely eaneel over a wide frequeney band.

The dimensions of the H-plane step required to eliminate the TE_{30} mode can be estimated by taking the Fourier transform of the aperture distribution. This method is open to eritieism as a teehnique for aeeurately determining the higher order modes generated at the discontinuity, but it appears to be a relatively easy method of representing the situation in a qualitative way. This analysis suggests that a ratio of $A/A' = 3/2$ (refer to Fig. 49) will suppress the TE_{30} mode. This is a highly desirable feature, beeause the presence of the TE_{30} mode would cause the H-plane patterns to be extremely sensitive to frequeney.

The $TE_{12} - TM_{12}$ degenerate pair required to produee a tapered aperture distribution in the E-plane may be generated by a symmetrieal diseontinuity in the E-plane. The step required for elimination of the TE_{30} mode for the other polarization is not, however, of the proper dimensions for this purpose, produeing not only the wrong excitation amplitude of $TE_{12} - TM_{12}$, but other undesired higher order modes as well. An abrupt taper in the E-plane with a transition to the larger reetangular waveguide will exeite the desired mode group. In order not to disturb the step, whieh is neeessary for suppression of the TE_{30} mode in the other polarization, the taper was eonstrueted using several fins. The dimensions were experimentally determined to give the desired result.

This eonfiguration is diffieult to analyze, particularly so in view of the faet that the fins are widely spaeed. The mode distributions obtained from pattern analysis suggest that the fins may

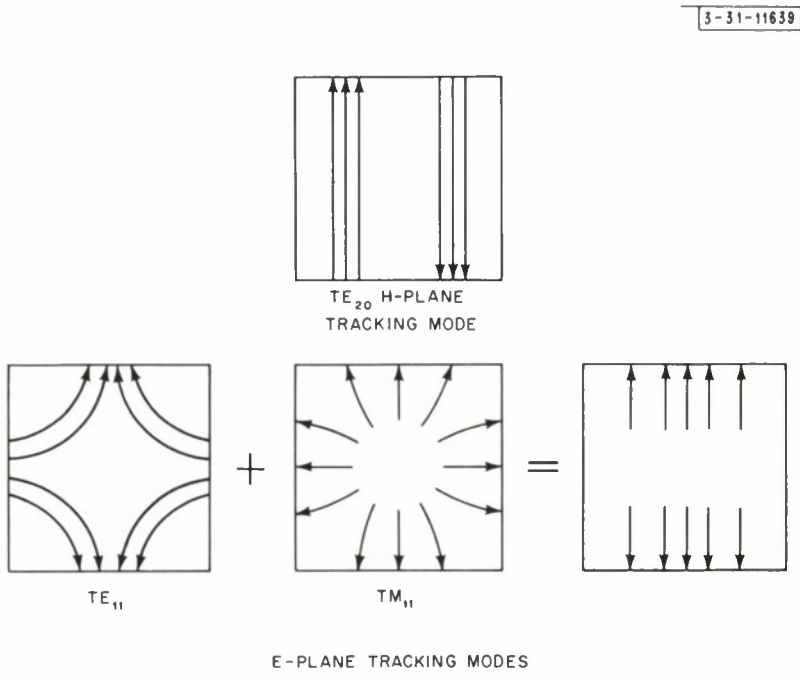

Fig. 48(b). Modes responsible for tracking beams.

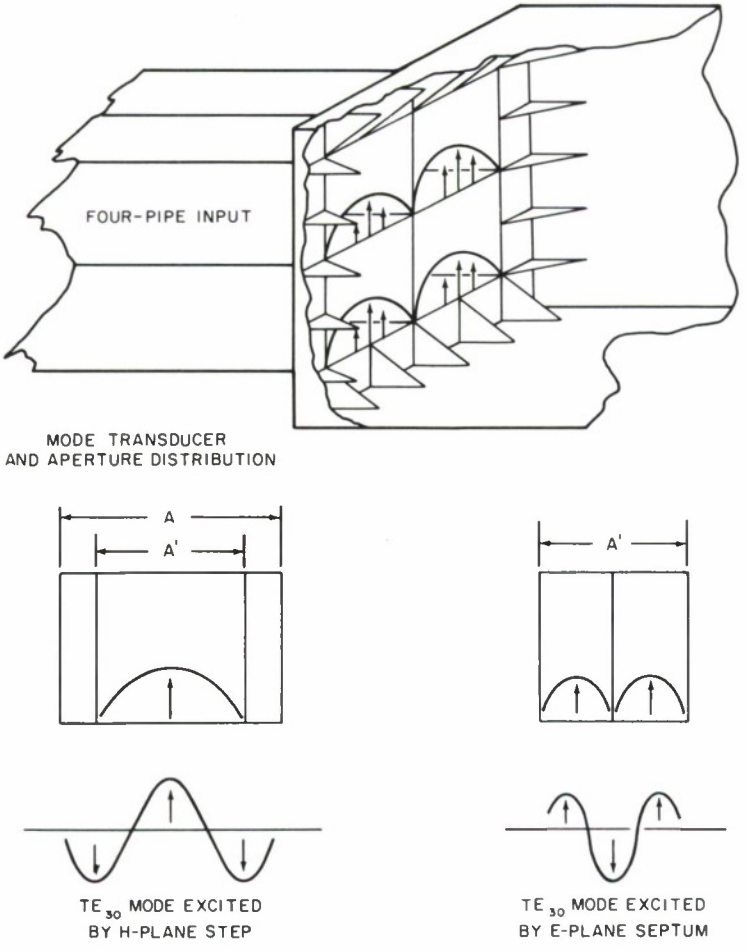

Fig. 49. Horn throat discontinuity and TE_{30} mode excitation.

be considered to represent a small step plus a moderately steep taper in the E-plane to a larger waveguide dimension. The present $TE_{12} - TM_{12}$ generator, Fig. 49, is probably not optimum, but does give good results in the sum beam over the frequency band of interest.

The conditions most favorable for the difference modes may be determined in much the same manner as for the sum modes. Analysis for the TE_{20} mode, for example, shows that the ratio $A/A' = 2$ will suppress the TE_{40} mode. This is considerably at variance with the requirements to eliminate the TE_{30} mode from the sum beam so it is not surprising that the H-plane difference patterns suffer some degradation by the strongly excited TE_{40} mode. A similar situation exists with respect to the E-plane difference patterns.

The present horn design does not allow independent control of all the modes required for the signal gathering and the monopulse tracking functions. Because tracking was not a requirement for the planetary radar, no attempt was made to introduce parameters which would provide additional control of the excitation of the tracking modes.

The various modes responsible for the aperture illumination travel at different velocities in the long pyramidal horn. In order to adjust the relative phases at the aperture, a section of waveguide of constant cross section was included and its length adjusted to give the best performance for the sum beam at the band center. Figure 50 shows the phase shift of several modes relative to the dominant TE_{10} for the 57λ-long pyramidal horn of Fig. 47.

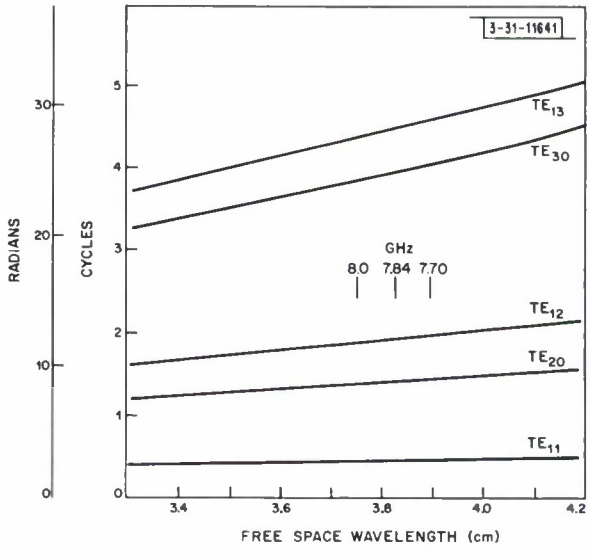

Fig. 50. Throat-to-operture shift of various modes relotive to TE_{10} dominant made for pyromidol horn.

In order to optimize the forward (sum) performance, the $TE_{12} - TM_{12}$ pair must be in phase at the aperture. The horn is two wavelengths longer for the TE_{10} mode than for the higher order mode pair. The frequency dependence of this differential phase shift causes the gain to fall off slowly on both sides of the design frequency. Fig. 50 points out the difficulty which would be experienced if the TE_{30} mode were present. In addition to the increased frequency dependence, it would be very difficult to adjust the TE_{30} phase with respect to the other necessary modes.

In the pyramidal horn the wave impedance is a function of the cross-sectional dimension of the horn and consequently the field amplitudes vary as the waves progress along the horn according to a relationship which is different from the 1/R of an expanding spherical wave.

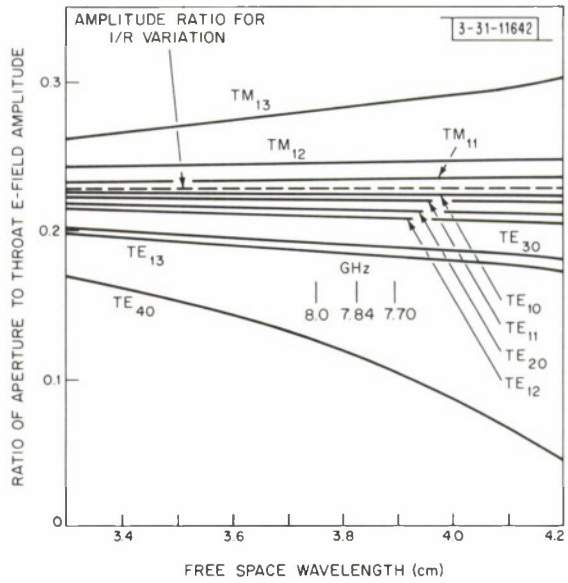

Fig. 51. E-field behavior for variaus modes in the lang pyramidal harn.

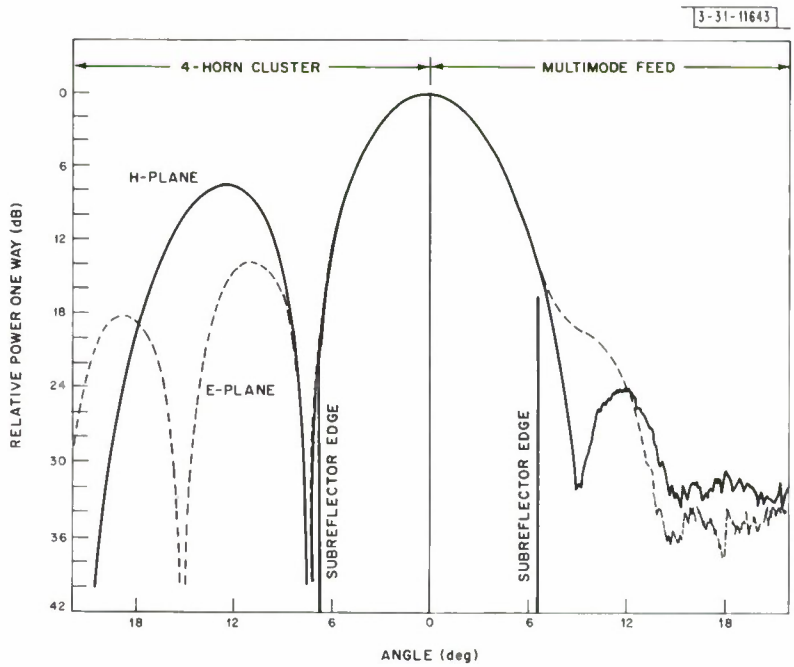

Fig. 52. Primary sum patterns – camparisan af faur-harn feed and multimade feed (measured).

The limiting case for very high frequencies is, of course, 1/R because here the wave impedance approaches the value of free space. The amplitude of TM modes will decrease less rapidly than TE modes (see Fig. 51). Consequently, degenerate mode pairs such as $TE_{12} - TM_{12}$ which were excited with equal amplitude at the horn throat will not be of equal amplitude at the aperture if one excludes the possibility of energy transfer between the components of the degenerate pair. The condition of unequal amplitude of the TE_{12} and TM_{12} modes at the aperture will result in a cross polarized component. Pattern measurements indicate that the cross polarization level is everywhere less than -23 dB from the peak of the main beam and is -40 dB on axis. This is of the order of magnitude expected from the data of Fig. 51.

H. Patterns and Pattern Analysis

The explanations of feed performance given up to this point indicate only that the distribution in the feed aperture will be a superposition of certain waveguide modes. The particular modes and their relative amplitudes depend upon the design of the mode launcher at the horn throat. The general nature of the horn throat makes the complete analysis difficult. However, the relative amplitudes and phases of the various modes actually existing at the horn aperture can be determined approximately by examining the radiation patterns.

A symmetrical excitation generates the forward or sum beam and for the most part excites the TE_{10} mode and the $TE_{12} - TM_{12}$ degenerate pair. However, there may be traces of TE_{30}, TE_{14}, TM_{14} and even TE_{50}. Of these the dominant TE_{10}, as well as the TE_{12}, TM_{12}, TE_{14} and TM_{14} modes, all have a distribution in the H-plane which can be represented by $\cos(\pi x/D)$, where D is the width of the feed aperture and $-D/2 \leqslant x \leqslant D/2$. The H-plane patterns are insensitive to the presence of these particular higher order modes. The effects of their presence will be felt in the E-plane patterns. The TE_{30} and TE_{50} modes have H-plane distributions which are respectively $\cos(3\pi x/D)$ and $\cos(5\pi x/D)$ with uniform E-plane distributions. Only the H-plane patterns are sensitive to the presence of these modes.

The experimentally determined H-plane pattern, Fig. 52, has beamwidths and sidelobe levels which, to a high degree of accuracy are predicted by the simple $\cos(\pi x/D)$ H-plane distribution. It can be concluded that the amounts of TE_{30} and TE_{50} present are negligible.

In the E-plane the dominant mode produces a uniform distribution whereas the TE_{12}, TM_{12}, TE_{14} and TM_{14} produce cosinusoidal distributions. The aperture distribution in the E-plane may be represented as

$$F(y) = C_0 + C_2 \left(\cos \frac{2\pi y}{D}\right) + C_4 \left(\cos \frac{4\pi y}{D}\right)$$

where $-D/2 \leqslant y \leqslant D/2$ and where C_0 accounts for the dominant mode, C_2 for the TE_{12}, TM_{12} degenerate pair and C_4 for the TE_{14}, TM_{14} degenerate pair. The corresponding radiation pattern is:

$$P(u) = C_0 \frac{\sin u}{u} + \frac{C_2}{2}\left[\frac{\sin(u-\pi)}{(u-\pi)} + \frac{\sin(u+\pi)}{u+\pi}\right] + \frac{C_4}{2}\left[\frac{\sin(u-2\pi)}{u-2\pi} + \frac{\sin(u+2\pi)}{u+2\pi}\right]$$

where $u = \pi D/\lambda \sin\Theta$, and Θ is the angle measured from the axis of the feed in the E-plane.

The pattern is expressed as the sum of terms of the form $\sin(u \pm n\pi)/u \pm n\pi$. These functions have a maximum value of unity and the useful property that at the maximum of any one

term the others are zero. This enables one to evaluate the constants C_2/C_0 and C_4/C_0 from the experimental patterns by selecting the values of u which maximize the individual terms. These values are $u = \mp n\pi$, and correspond to the angular position $\theta_n = \mp \sin n\lambda/D$.

The results of the analysis show that $C_2/C_0 \cong 0.45$ to 0.5. This is just the amount of TE_{12}, TM_{12} required to equalize the principal plane beamwidths. The ratio C_4/C_0 is approximately 0.2 and represents the undesired mode pair, TE_{14}, TM_{14}, responsible for the −20-dB shoulders in the E-plane pattern (see Fig. 52).

There are two different antisymmetrical conditions which lead to the tracking patterns. Antisymmetric excitation in the E-plane leads to mode pairs such as TE_{11}, TM_{11} and TE_{13}, TM_{13}. The mode pair TE_{13}, TM_{13} is undesirable but unfortunately it is generated strongly and the phase of this higher mode pair at the aperture plane varies quite rapidly with respect to that of the TE_{11}, TM_{11} pair. Much of the energy in these higher order modes is spilled over, i. e., not intercepted by the subreflector in the Cassegrainian antenna system. Because of the rapid phase variation with respect to the TE_{11}, TM_{11} pair, there is a narrow-banding effect and a loss in tracking efficiency. This is partially offset by the superior on-axis gain of the feed, and results in a tracking capability which is comparable to that obtained using a four-horn cluster.

The distribution in the E-plane for E-plane tracking is

$$F(y) = A_1 \sin\left(\frac{\pi y}{D}\right) + A_3 \sin\left(\frac{3\pi y}{D}\right)$$

where the first term represents the TE_{11}, TM_{11} mode pair and the second term the TE_{13}, TM_{13} pair. The pattern is given by:

$$P(u) = A_1 \left[\frac{\sin(u - \pi/2)}{(u - \pi/2)} - \frac{\sin(u + \pi/2)}{(u + \pi/2)}\right] + A_3 \left[\frac{\sin(u - 3\pi/2)}{(u - 3\pi/2)} - \frac{\sin(u + 3\pi/2)}{(u + 3\pi/2)}\right] .$$

The same technique employed in the analysis of the sum patterns was used to determine the ratio A_3/A_1 to be approximately 1.4.

For the other remaining pattern, which is antisymmetrical in the H-plane but symmetrical in the E-plane, it is sufficient to consider the TE_{20} and TE_{40} modes. In this case, once again, the higher order TE_{40} is undesirable, since it leads principally to spilled-over energy. It is quite strongly excited and its phase at the aperture varies rapidly with frequency with respect to the TE_{20} mode. In this case, just as in the E-plane antisymmetric case, the presence of the higher mode tends to degrade the tracking characteristic. The tracking pattern in the H-plane is represented by

$$P(u) = B_2 \left[\frac{\sin(u + \pi)}{(u + \pi)} - \frac{\sin(u - \pi)}{(u - \pi)}\right] + B_4 \left[\frac{\sin(u + 2\pi)}{(u - 2\pi)} - \frac{\sin(u - 2\pi)}{(u - 2\pi)}\right]$$

where the quantity B_4/B_2 represents the ratio of the TE_{40} mode to the TE_{20} mode and is found to be approximately 0.6.

A factor of considerable importance in both of these cases of antisymmetry is the phase of the monopulse sum signal relative to each monopulse difference signal. The feed is quite broadbanded in this respect if only the desired tracking modes exist, since there is little relative phase shift between TE_{10} and the TE_{11}, TM_{11} pair and it is not a large effect between TE_{10} and TE_{20}.

The presence of the undesired higher order modes produces frequency sensitive phase variations between the sum and difference channels in addition to having an effect on the tracking patterns and on tracking sensitivity. Reduction of the amplitude of the TE_{13} and TM_{13} and TE_{04} modes would improve both the difference beam characteristics and the tracking efficiency. Experimentation with the mode generator was not carried far enough to suggest how this might be accomplished without degrading the sum beam characteristics.

The primary sum patterns obtained for the multimode horn are shown on the right in Fig. 52, and compared to those obtained for a conventional four-horn cluster on the left. The patterns have been normalized to the same gain at the peak of the beam thus obscuring the fact that the beam efficiency for the multimode horn is about 1.4 dB greater than for the four-horn cluster. The secondary patterns of the Haystack antenna using the multimode feed are shown in Fig. 53.

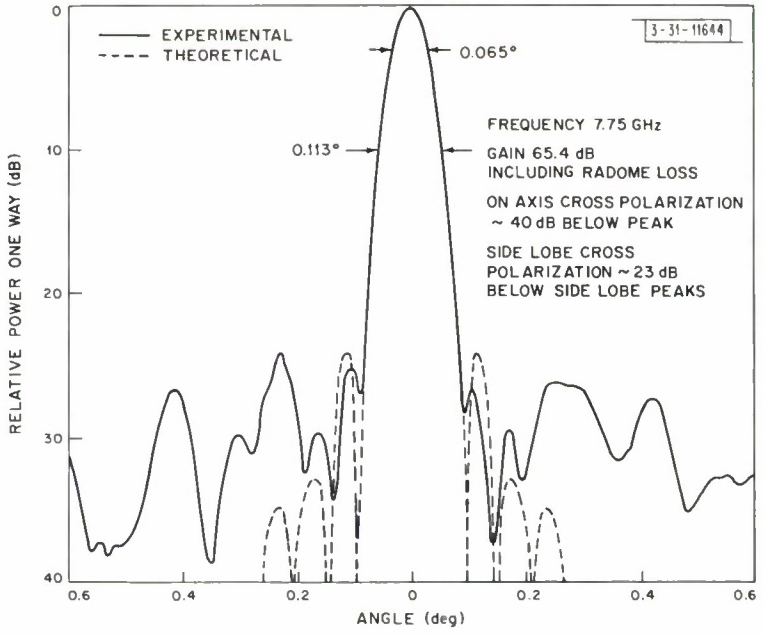

Fig. 53. Haystack secandary patterns with multimade feed receiving left circular palarizatian.

The superior quality of the feed is also illustrated by antenna temperature measurements made using a radiometer. Figure 54 compares Haystack antenna temperatures measured using thc multimode feed with data taken using a Clavin feed[39] which had been designed and used as a low-noise radiometer feed. The difference between the 8.25 GHz of the radiometer feed and the 7.75 GHz of the multimode feed would be responsible for a negligible difference in the effective antenna temperature.

The beam efficiency of a Cassegrainian feed is defined as the percentage of the total power radiated which is directed at the subreflector. Calculations based on the aperture distribution, neglecting the small amount of undesired higher order modes, give a beam efficiency of 95 to 96 percent. Integration of the measured E- and H-plane patterns making the usual assumptions regarding symmetry and using the measured primary gain, gives a figure of about 90 percent. The Haystack antenna has been the subject of very intensive studies from which it has been determined that the surface tolerance loss is 0.8 dB and the radome loss 1.2 dB at a frequency of 7.75 GHz. The measured gain of the antenna is 65.4 ± 0.5 dB which, when corrected for radome

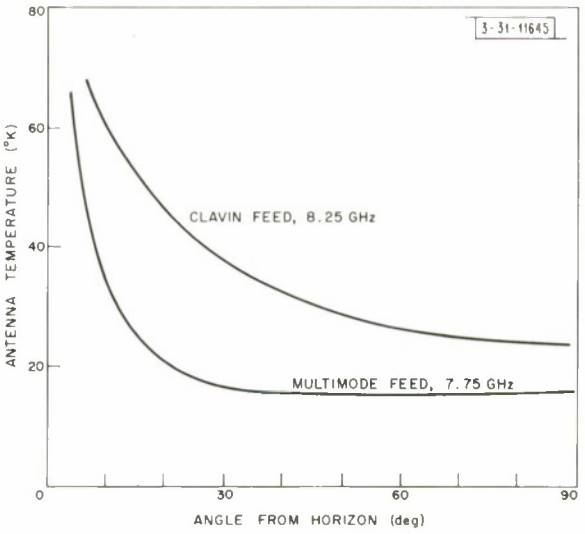

Fig. 54. Haystack antenna temperature using various feeds.

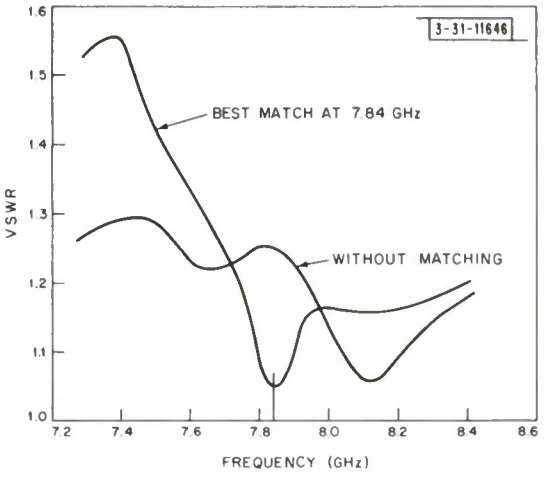

Fig. 55. Impedance characteristic of Haystack feed (does not include OMT and polarizer).

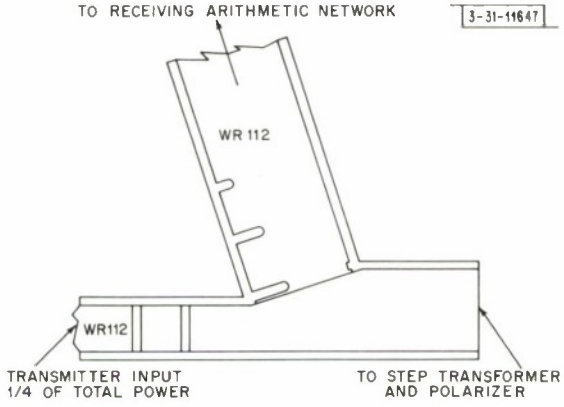

Fig. 56. One element of OMT assembly.

and tolerance loss, gives a gain value of 67.4 ± 0.5 dB and an efficiency of 62.4 ± 7.2 percent. This is consistent with a value of feed efficiency of 90 percent.

The multimode feed, with no matching device whatever, has a VSWR no greater than 1.24 over the entire band from 7.6 to 8.4 GHz, but under these conditions the VSWR is 1.22 at 7.84 GHz. For this reason, a small symmetrical iris has been placed in each square waveguide 2.66λ behind the throat aperture. The performance of the feed with the iris is shown in Fig. 55. The VSWR is better than 1.1 for a bandwidth of more than 100 MHz centered on a frequency of 7.84 GHz, the planetary radar frequency.

The feed aperture is covered with a thin radome fabricated from polyethylene sheet. This radome does not alter the feed characteristics. Its purpose is to keep foreign material out of the microwave system and allow pressurization of the system to up to 1 psi in order to prevent condensation of moisture inside the waveguide.

I. OMT (Orthogonal Mode Transducer) and Circular Polarizer

One of the simplest ways of generating circular polarization where polarization diversity, i. e., rapid change of polarization characteristic, is not a requirement is to use an OMT which allows injection of two orthogonal linear polarizations into a waveguide of symmetrical cross section, i. e., either square or circular. This is followed by a microwave equivalent of the quarter wave plate which will produce circular polarization, the sense of circularity being dependent upon which of the two possible linear polarizations is incident upon the polarizer. In the Haystack monopulse system, each of the four waveguides feeding the multimode horn contains an OMT and polarizer. These components were carefully constructed using electroforming techniques to insure that the four transmission paths are as identical as is achievable within reason. Figure 56 is a longitudinal cross section of a typical OMT.

The OMT was designed with its orthogonal inputs in WR-112 waveguide and with a step transformer to match the orthogonal mode section into the 0.990-inch square waveguide of the circular polarizer. This size of square waveguide was chosen for the polarizer in order to insure that the TE_{11} mode was cut off below 8.2 GHz. This design was a concession to radiometry. An earlier polarizer in 1.122-inch square waveguide had exhibited small resonance absorptions due to presence of the TE_{11} mode which could not be radiated because of the horn throat dimensions. These resonances were so positioned that they produced no adverse effect on the planetary radar performance, but they did interfere with radiometer experiments designed to detect helium lines.

The circular polarizer[40] design is shown in Fig. 57 and its differential phase shift characteristic in Fig. 58. In the design used in the planetary radar system, the step transformer was adjusted to provide the best match for the OMT-polarizer assembly. This is shown in Fig. 59.

The construction of the OMT and polarizer of electroformed copper has reduced the insertion loss to a minimum. The loss for the OMT through the side arm, which is the normal received signal path, has been determined to be less than 0.02 dB. This loss is somewhat higher than the loss of an equivalent length of copper waveguide, partly due to the inductive matching elements required to remove the 2:1 mismatch of the unmatched junction. The loss in the circular polarizer has been determined to be 0.012 dB.

The power handling ability of this assembly is limited by the OMT. Breakdown of an OMT unit occurred at 272 kW CW when operated in an unpressurized traveling wave resonator. This measurement was made by connecting two OMT units (see Fig. 56) back to back and passing high power through the "thru" ports which represents the conditions of use in the Haystack system.

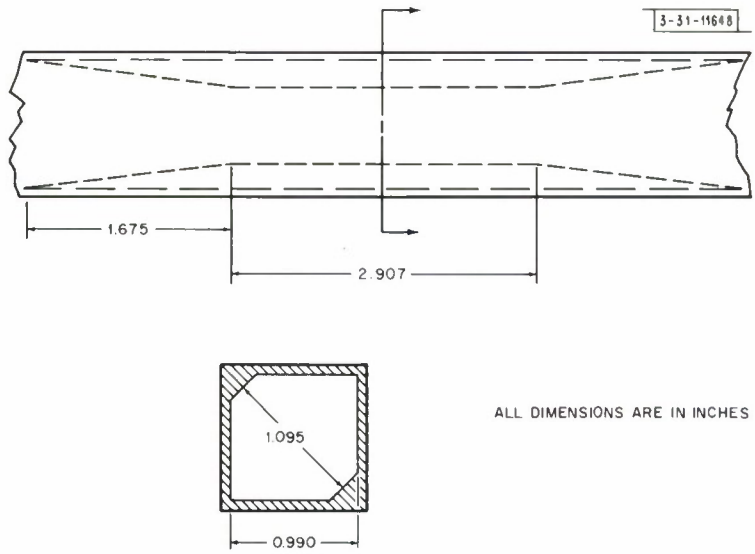

Fig. 57. Circular polarizer.

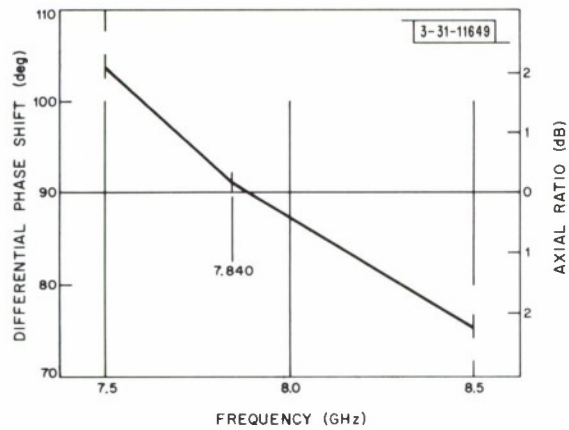

Fig. 58. Perfarmance of circular palarizer.

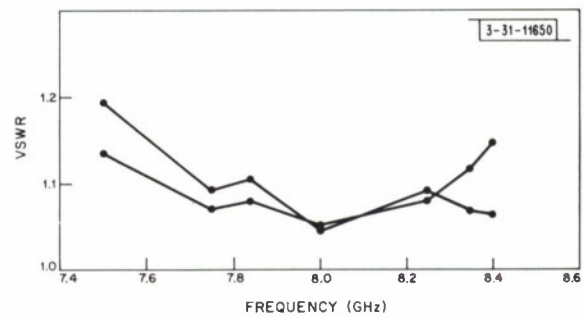

Fig. 59. VSWR af OMT polarizer assembly.

VII. PROTECTION OF THE HIGH POWER RF SYSTEM

An expensive sophisticated remotely operated piece of equipment, such as the planetary radar, must be provided with a protective system which is capable of minimizing damage when a fault occurs. This protective system must be designed so that information on the nature of the fault and its location is preserved in order that the causes of the failure can be diagnosed and the proper corrective measures taken. Without a well-designed protective system, it is questionable whether a 500-kW CW microwave system at X-band could be deployed successfully. The protective system in the planetary radar was designed to provide continuous monitoring of all critical areas, to automatically initiate shutdown at the proper level whenever a fault should occur, and to provide an indication of fault location even if a complete power failure accompanied the fault.

The need for making provision for the protection of the microwave system from catastrophic failure, due to a malfunction, is much more important for the case of a CW than for a pulsed system because the CW mode of operation does not have built into it the periodic shut-off feature inherent in the pulsed system. This is not to say that pulsed systems might not need fault protection, but the problem is not viewed with as much urgency. In a CW microwave system there are three electrical fault situations which require immediate protective response. These are (a) an arc in the transmission line, (b) a multipactor discharge occurring on the vacuum side of the RF output window of the transmitter tube, and (c) interception of an excessive number of high energy electrons by the drift tube section of the klystron amplifier or by the RF structures in the case of a high power traveling wave tube. In addition to these, there are requirements on the fluid coolant and other environment determining factors which must be interlocked in such a way as to prevent a catastrophic situation from developing.

Figures 2 and 11 show the location of sensors associated with the high power microwave transmission system. In addition, there are sensors with fault thresholds to detect excess body current in the klystron and to detect changes in the field of the focusing electromagnet. The output of these sensors is fed into a Fault Logic Unit (FLU) which (a) initiates the proper sequence of events to shut down the transmitter, and (b) operates indicating lamps so that the system operator can determine the location of the fault and diagnose the problem.

The fault system employed has a great deal of redundancy which was built in by design. An arc in the waveguide, for example, could be detected by any one or all of the following sensors: (a) optical arc detector, (b) reverse power detector, (c) line unbalance detector, and (d) forward power detector. It was not possible, however, to always arrive at this degree of redundancy. An intense multipactor discharge on the vacuum side of the window, which if undetected would destroy the window, is sensed with certainty only by the optical arc detector which is positioned to have the window in its field of view. In principle, one might expect that such a fault would also be seen by the line unbalance detector, but operating experience has not shown this to be the case.

The operation of the FLU is illustrated by the diagram on Fig. 60. This unit controls the RF excitation of the 500-kW klystron transmitter in accordance with the status of signals derived from protective and interlock circuits in the RF box. In addition, it receives signals and timing pulses from the pulse coordinator. These timing signals, plus those generated within the fault logic unit as a result of inputs from the fault sensors, control both the RF excitation and the DC

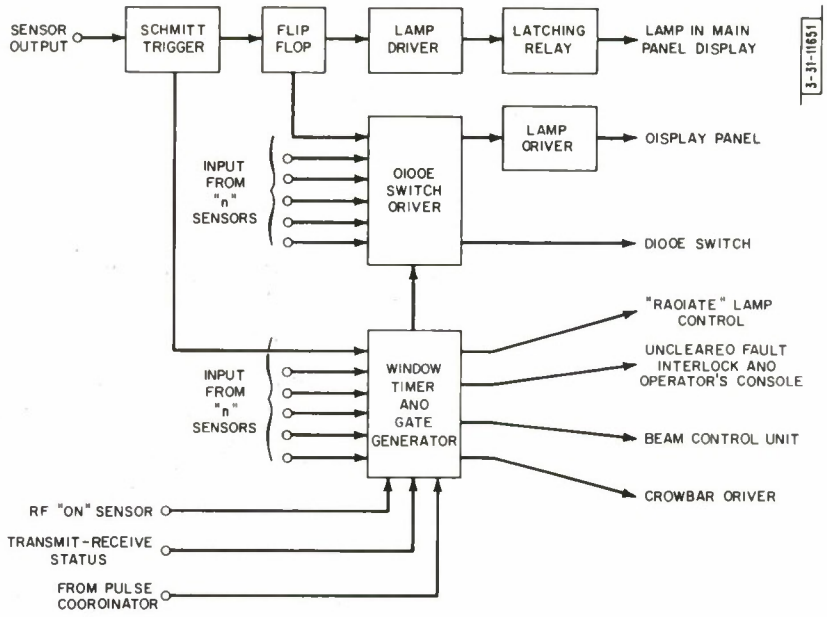

Fig. 60. Simplified diagram of fault logic unit.

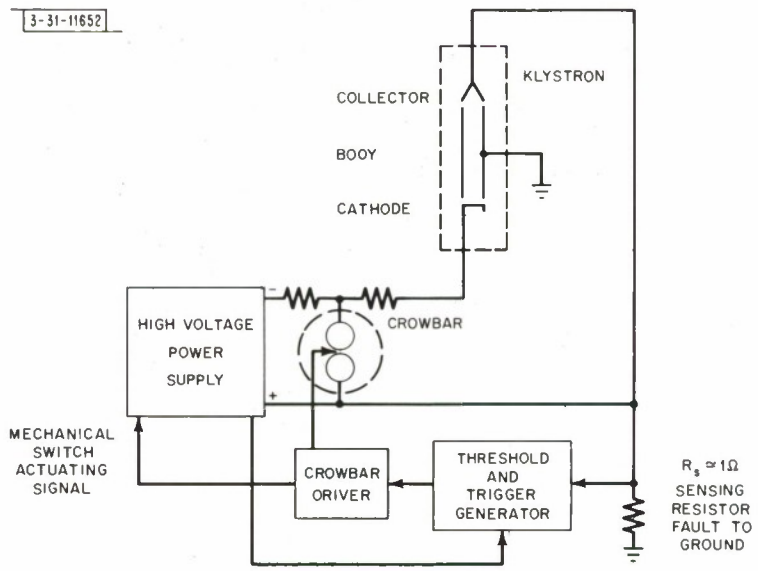

Fig. 61. Basic connection of crowbar and high voltage power supply.

or video voltages applied to the beam control element of the klystron amplifiers. Control of the RF excitation is accomplished by means of PIN diode switches in the RF drive network. The klystron beam is controlled by a voltage developed in the Beam Control Unit (BCU). Pulses which control the status of the BCU are routed through the FLU where they are regenerated and fed to the BCU in accordance with the fault status.

The diode switch driver generates the current waveform which is used to drive the PIN diode attenuator. In the case of an RF fault, the RF drive to the klystron is reduced to the point where the RF output is not large enough to sustain further damage due to RF effects. The shut-off of RF drive occurs in the order of one μsec. The PIN diode switches are designed to be fail safe, that is, maximum attenuation occurs for zero diode current. However, if a diode fails through short circuiting of the diode junction, which is perhaps the most likely type of PIN diode failure, the attenuation of the switch is reduced by substantially the attenuation contributed by that diode.

In the event that the PIN diode switch fails to reduce the RF output within 10 μsec, the window timer will cause a stop pulse to be generated and applied to the BCU which will cut off the beam in about 3 μsec. An option is also provided to send a locally generated trigger to the crowbar [41] circuit which will shut down and discharge the high voltage power supply.

It is desirable to preserve a knowledge of the location of a fault even though all power associated with the transmitter is lost. For this reason latching relays have been incorporated in all of the fault sensing circuits. This allows preservation of the fault sensor readouts in case of a power failure and allows determination of the true cause of the failure which otherwise might not be traceable.

DC faults both within and external to the high voltage power supply are sensed and the appropriate drive signals generated to disconnect the power supply from the AC mains and to discharge the capacitor bank. From the standpoint of the RF system, the interest is in the protection afforded by the crowbar to the klystron should the body of the tube suddenly begin to intercept an abnormal amount of the beam current either due to a "gas burst" within the vacuum envelope, a failure of the magnet power supply, or a failure of the focusing magnet itself. The crowbar discharges and shuts down the high voltage DC supply in less than 10 μsec from the time a trigger is generated in the FLU. When an RF fault exists the crowbar is fired only if the diode switches fail to remove the RF, or if the BCU fails to cut off the klystron beam. Figure 61 shows the manner in which the power supply and crowbar are connected in the Haystack system. Any fault to ground, be it via the klystron or a human body, will cause current to flow in the sensing resistor shown in Fig. 61. When the set threshold is exceeded, the crowbar will be fired, discharging the supply. It has been accidentally demonstrated that this fast crowbar can forgive an ordinarily fatal mistake. However, it is not recommended that this be a substitute for safety procedures.

ACKNOWLEDGMENTS

The work reported in this paper was made possible by the combined efforts of a large number of people. I am particularly indebted to the following individuals: W. A. Andrews, A. A. L. Browne, G. L. Davidson, F. J. Dominick, O. K. Downs, W. D. Fitzgerald, R. V. Keating, K. J. Keeping, A. H. Kessler, E. P. McCurley, C. E. Muehe, C. A. Peterson, A. F. Standing, and especially to M. L. Stone, who shouldered much of the responsibility, making certain that the microwave system would be compatible with the sophisticated Haystack antenna and radar systems.

REFERENCES

1. I.I. Shapiro, "Fourth Test of General Relativity," Phys. Rev. Letters 13, 789 (1964), DDC 613894.
2. _____, "Effects of General Relativity on Interplanetary Time-Delay Measurements," Technical Report 368, Lincoln Laboratory, M.I.T. (1964), DDC 614232.
3. _____, "Fourth Test of General Relativity: Preliminary Results," Phys. Rev. Letters 20, 1265-1269 (1968), DDC 673608.
4. H.G. Weiss, "The Haystack Experimental Facility," Technical Report 365, Lincoln Laboratory, M.I.T. (1964), DDC 608272.
5. J. Jasberg and J.V. Lebacqz, "High Power Microwave Windows," SLAC-PUB-49, Stanford Linear Accelerator Center, Stanford University (1964).
6. R.W. Bierce, W.R. Fowkes, and J.H. Jasberg, "Window Materials Design and Properties for Use in High Power Klystrons," SLAC-PUB-92, Stanford Linear Accelerator Center, Stanford University (1965).
7. R.M. Weigand, "RF Generated Shock Waves," Proc. IEEE Letters 54, 1485-1486 (1966), DDC 649352.
8. D.H. Preist and R.C. Talcott, "On the Heating of Output Windows of Microwave Tubes by Electron Bombardment," Trans. IRE PGED ED-8, 243-251 (1961).
9. F. Paschke, "Heating of Waveguide Windows as a Limit to the Output Power of Microwave Tubes," RCA Review 23, 311-322 (1962).
10. C.E. Muehe, "Some Aspects of High Power Window Design," Group Report 46G-0003, Lincoln Laboratory, M.I.T. (1960), DDC 244326.
11. _____, "Thermal Cracking of Waveguide Windows," Technical Note 1966-19, Lincoln Laboratory, M.I.T. (1966), DDC 628907.
12. L. Gould, Handbook on Breakdown of Air in Waveguide Systems, Index No. NE111616, Navy Dept., Bu. Ships, Electronics Div., Contract Nobsr 63295, April 1956.
13. L.J. Milosevic and R. Vautey, "Traveling-Wave Resonators," Trans. IRE PGMTT MTT-6, 136-143 (1958).
14. S.J. Miller, "Traveling Wave Resonator and High Power Testing," Microwave Journal 3, 50-58 (1960).
15. A.A.L. Browne, "The Feasibility of Locating Waveguide Arcs by Sound Ranging," Trans. IEEE PTGMTT MTT-16, 894 (1968).
16. Reference Data for Radio Engineers, H.P. Westman, Ed. (ITT Corp., New York, 1964), 854.
17. J.W.S. Rayleigh, The Theory of Sound (Dover, New York, 1945), Vol. II, Par. 347.
18. A. Wood, Acoustics (Dover, New York, 1966).
19. S.C. Lin and G.P. Theofilos, "Hydrodynamic Effects Produced by Pulse Microwave Discharges," Physics of Fluids 6, 1369-1381 (1963).
20. J.D. Krauss, "Recent Advances in Radio Astronomy," IEEE Spectrum 1, 78-95 (1964).
21. H.P. Taylor, "The Radiometer Equation," Microwave Journal 10, 39-42 (1967).
22. K.M. Eisle, "Refrigerated Microwave Noise Sources," Trans. IEEE PTGIM IM-13, 336-342 (1964).
23. T. Mukaihata, B.L. Walsh, M.F. Bottjer and E.B. Roberts, "Subtle Differences in System Noise Measurements and Calibration of Noise Standards," Trans. IRE PGMTT MTT-10, 506-516 (November 1962).
24. D. Merlo, E.W. Houghton and G.J. Halford, "Effect of Some Component Tolerances and Measuring Errors on Noise Measurements," Electronics Letters 1, 250-251 (1965).
25. A.E. Siegman, Microwave Solid-State Masers (McGraw-Hill, New York, 1963).

26. C.T. Stelzriec, "A Liquid-Helium Cooled Coaxial Termination," Proc. IRE 49, 1224 (1961).

27. A.A. Penzios, "Helium Cooled Reference Noise Source in a 4 kmc Waveguide," Rev. Sci. Instruments 36 (1) (1965).

28. C.E. Muehe and A.A.L. Browne, "X-Band Gas Tube Pulsed Attenuator for Maser Protection" (to be published in Trans. IEEE).

29. L.J. Ricardi and L. Niro, "Design of a Twelve Horn Monopulse Feed," IRE Internatl. Conv. Record 9 (1), 49 (1961).

30. W.D. Fitzgerald, "Comparison of Cassegrain Tracking Feeds" (to be published in Trans. IEEE).

31. K.J. Keeping, "Design and Construction of a Multimode Circularly Polarized Monopulse Tracking Feed for High Power Application in a Cassegrain Reflector System," IEEE Convention Record 13 (5), 101-109 (1965).

32. S.W. Drabowitch, "Multimode Antennas," Microwave Journal 9, 41-51 (1966).

33. P.D. Potter and A.C. Ludwig, "Beam Shaping by Use of Higher Order Modes in Conical Horns," NEREM Record 5, 92-93 (1963).

34. P.A. Jensen, "A Low-Noise Multimode Cassegrain Feed with Polarization Diversity," NEREM Record 5, 94-95 (1963).

35. V.V. Galindo and C.Y. Pon, "Control and Optimization of a Multimode Square Feed for Sum and Difference Patterns," NEREM Record 5, 96-97 (1963).

36. P. Foldes and S. Komlos, "A New Multimode Monopulse Feed," NEREM Record 5, 100-101 (1963).

37. K.J. Keeping, "Early Test Results with the Circularly Polarized Tracking Feed in the Haystack Antenna," NEREM Record 7, 18 (1965).

38. S. Silver, Microwave Antenna Theory and Design (McGraw-Hill, New York, 1949), pp. 377-380.

39. A. Chlavin, "A New Antenna Feed Having Equal E and H Plane Patterns," Trans. IRE, PGAP AP-2, 113-119 (1954).

40. A.H. Kessler and W.J. Getsinger, "A Simplified Method for Designing an Elliptical Polarizer in Square Waveguide," Group Report 46G-3, Lincoln Laboratory, M.I.T. (1963), DDC 407624.

41. A.J. Morris and J.P. Swanson, "High Speed Protection of Microwave Tubes and Systems," Microwave J. 5 (11), 78-85 (1962).

DOCUMENT CONTROL DATA – R&D

(Security classification of title, body of abstract and indexing annotation must be entered when the overall report is classified)

1. ORIGINATING ACTIVITY *(Corporate author)* Lincoln Laboratory, M.I.T.	2a. REPORT SECURITY CLASSIFICATION Unclassified 2b. GROUP None

3. REPORT TITLE

The Microwave System of the Haystack Planetary Radar

4. DESCRIPTIVE NOTES *(Type of report and inclusive dates)*

Technical Report

5. AUTHOR(S) *(Last name, first name, initial)*

Jones, Clarence W.

6. REPORT DATE 23 October 1968	7a. TOTAL NO. OF PAGES 72	7b. NO. OF REFS 41
8a. CONTRACT OR GRANT NO. AF 19(628)-5167 b. PROJECT NO. 649L c. d.	9a. ORIGINATOR'S REPORT NUMBER(S) Technical Report 457 9b. OTHER REPORT NO(S) *(Any other numbers that may be assigned this report)* ESD-TR-68-329	

10. AVAILABILITY/LIMITATION NOTICES

This document has been approved for public release and sale; its distribution is unlimited.

11. SUPPLEMENTARY NOTES None	12. SPONSORING MILITARY ACTIVITY Air Force Systems Command

13. ABSTRACT

The microwave system of the Haystack Planetary Radar is described and performance data presented. A detailed description of techniques and components is included for those cases which are not representative of common usage or where the state of the art has been advanced.

14. KEY WORDS

Haystack	ferrite circulator	gas attenuator
X-band planetary radar	maser	circular polarizer
high power microwave transmission	traveling wave resonator	multimode horn